Time-Lapse Imaging

Erik Meijering, Ihor Smal, Oleh Dyubachyk,

Jean-Christophe Olivo-Marin

Original unedited version of

Chapter 15 of *Microscope Image Processing*

Q. Wu, F. A. Merchant, K. R. Castleman (eds.)

Elsevier Academic Press, 2008, pp. 401-440

INTRODUCTION

By their very nature, biological systems are dynamic, and a proper understanding of the cellular and molecular processes underlying living organisms and how to manipulate them is a prerequisite to combat diseases and improve human health care. One of the major challenges of current biomedical research, therefore, is to unravel not just the spatial organization of these complex systems, but their *spatiotemporal* relationships [142,42]. Catalyzed by substantial improvements in optics hardware, electronic imaging sensors, and a wealth of fluorescent probes and labeling methods, light microscopy has, over the past decades, matured to the point that it enables sensitive time-lapse imaging of cells and even single molecules [150,93,166,100]. These developments have had a profound impact on how research is currently being conducted in the life sciences.

An inevitable consequence of the new opportunities offered by these developments is the fact that the size and complexity of image data is ever increasing. Nowadays, data sets generated in time-lapse experiments commonly comprise hundreds to thousands of images, each containing hundreds to thousands of objects to be analyzed (see Figure 1 for examples). Needless to say, such huge amounts of data cannot be digested by visual inspection or manual processing within any reasonable amount of time. It is now generally recognized that automated methods are necessary, not only to handle the growing rate at which images are acquired, but, possibly even more importantly, to provide a level of sensitivity and objectivity that human observers cannot match [97,41].

Roughly speaking, time-lapse imaging studies consist of four successive steps: 1) planning of the experiment and acquisition of the image data, 2) preprocessing of the data to correct for systemic as well as random errors and to enhance relevant features, 3) analysis of the data by detecting and tracking the objects relevant to the biological questions underlying the study, and 4) analysis of the resulting trajectories to test predefined hypotheses or detect new phenomena. This chapter addresses each of these issues (see Figure 2 for a topical overview), from an informatics perspective. It focuses on methodological rather than hardware or software aspects. It gives examples of image processing and analysis methods that have been used successfully for specific applications. The ultimate goal of this chapter is to prepare the reader to select methods intelligently.

IMAGE ACQUISITION

Time-lapse imaging experiments involve the acquisition of not only spatial information, but also temporal information, and often spectral information as well, resulting in up to five-dimensional (5D) image data sets (Figure 3). Regardless of the imaging technique used, a careful design of the microscope setup is imperative, as shortcomings may require additional pre- or postprocessing of the resulting image data or, worse, may lead to artifacts that cannot be removed and that may hamper data analysis. While it is outside the scope of this chapter to provide detailed guidelines for establishing the right setup, a few general remarks are made here, concerning the choice of microscopy, spatial dimensionality, and temporal resolution, from the perspective of subsequent data analysis.

Microscope Setup

A fundamental concern in time-lapse imaging experiments, which generally involve living cells and organisms, is to keep the specimen alive during the acquisition of hundreds or thousands of images over an extended period of time, ranging from minutes to hours, depending on the research question. This not only calls for a suitable environment, with controlled temperature, humidity, and a stably buffered culture medium [49], it also requires economizing light exposure, as living cells are sensitive to photodamage [133]. In the case of fluorescence microscopy, illumination bleaches fluorophores, which limits their emission time span and generates free radicals that are toxic for cells.

From an image analysis perspective, on the other hand, two very important factors that determine whether automated methods can be successfully applied, and that strongly affect their accuracy, are signal contrast (the difference in intensity between objects and background) and noise (which in light microscopy is signal dependent). These two factors are usually combined into a single measure: the signal-to-noise ratio (SNR). Ideally, experiments should be designed so as to maximize this measure in order to allow robust and accurate automated image analysis, and the only way to accomplish this would be to maximize light exposure and capture.

These contradictory requirements call for a careful choice of the type of microscopy to be used. This also depends on the type of objects to be studied, their dimensions, motility, and viability. Living cells in culture media, for example, produce poor contrast with standard brightfield illumination and often require contrast enhancing imaging techniques, such as phase-contrast or differential interference contrast microscopy. Intracellular particles are hardly (if at all) visible without contrast enhancement and are better studied using fluorescence microscopy (cf. Tables 1 and 2). Needless to say, in all cases the system should make the best possible use of the available light, implying the use of high numerical aperture objectives in conjunction with highly sensitive detectors. In many cases this may also mean that widefield microscopy is preferable over confocal microscopy [133,49,78], with the proviso that 3D widefield microscopy requires images to be deconvolved.

In practice, for any biological application, there is often no single best microscope setup. This means that a compromise will have to be found between sufficient (but not toxic) illumination, and (spatial and temporal) resolution, so that the maximum number of acceptable images (optical slices and time frames) can be acquired before the specimen is completely photobleached or damaged [49], where “acceptable” means having the minimum SNR required by automated image analysis techniques (discussed later in this chapter). To this end, a good understanding of different microscope systems is needed, for which we refer to excellent introductory texts [100].

Spatial Dimensionality

One of the fundamental questions to be addressed when setting up an experiment is whether imaging needs to be performed in two or in three spatial dimensions over time (denoted as 2D+t and 3D+t, respectively, the latter of which is also referred to as 4D). Despite the 4D imaging buzz in the literature, the vast majority of experiments today are still performed in 2D+t (cf. Tables 1 and 2). Often, this is due to limitations imposed by photobleaching and phototoxicity, which do not permit wasting light signal, as occurs in confocal microscopy imaging. In other studies, in particular those addressing intracellular dynamic processes, acquiring multiple optical slices would simply take too much time relative to the motions of interest, resulting in intrascan motion artifacts. In some cases, for example when studying cell migration in monolayers [64], or microtubule dynamics in neurons [132], the structures of interest may be sufficiently flat to allow 2D+t imaging by widefield microscopy to give a good understanding of a process. The improved light collection and the lower number of optical slices in such cases yields a better SNR and allows for higher temporal resolution.

Most cellular and intracellular processes, however, occur in three dimensions over time, and require 3D+t imaging in order to obtain a complete picture and fully characterize cell morphodynamics [133]. It is known, for example, that tumor cells treated with drugs that block migration on 2D substrates can move inside an artificial 3D collagen matrix by means of a very different type of motility [152,166]. Regarding intracellular processes, studies into kinetochore microtubule dynamics [35] have recently revealed that trajectories obtained from 2D+t imaging may differ significantly from those obtained from 3D+t imaging and may lead to severe misinterpretation of the underlying processes. These findings suggest that a paradigm shift may be necessary, in that 2D+t imaging studies should always be preceded by 3D+t experiments confirming their validity. This could be as important as making sure that fluorescent probes, in fluorescence microscopy imaging, do not alter physiology.

Temporal Resolution

Another issue of great importance in time-lapse experiments is the rate at which images should be acquired over time, also referred to as the temporal sampling rate, or temporal resolution. Ideally, this should be sufficiently high to capture the relevant details of object motion. However, similar to spatial dimensionality and resolution, the temporal sampling rate is not an independent parameter that can be fixed to any desired value, but is constrained by the limited viability of living cells under illumination. Nevertheless, in view of eventual data analysis, it is important to be aware of possible discrepancies between theoretically desirable and practically feasible values.

From sampling theory [123] it is known that in order to be able to reconstruct a continuous signal from a digitized version of it, the latter must have been acquired by sampling at a rate that is at least twice the maximum frequency component contained in the former. Similar to sampling in space (discussed in detail elsewhere in this volume), this rate, often called the Nyquist rate, also applies to sampling in time: true object position as a function of time is a continuous signal, and high-fidelity reconstruction of this signal and any derivative motion parameters, such as velocity and acceleration, is possible only if sampling is done at a rate that complies with theory.

Establishing this rate, however, is a chicken-and-egg problem: before sampling, one must already have knowledge of the velocities to be estimated, which can only be obtained by sampling at a proper rate in the first place. In practice, a series of experiments at different sampling rates will often be necessary to arrive at the optimal setting. Several studies can be found in the literature [70,84,35] that discuss temporal resolution for specific applications and that clearly demonstrate how undersampling may have a

significant effect on velocity estimation. From the point of view of image analysis it should also be realized that many automated cell tracking algorithms (cf. Table 1) fail if the displacement between time frames is larger than the cell diameter [166], especially in the case of cell contact. Similar limitations exist for particle tracking algorithms (cf. Table 2) in the case of high densities or when trying to characterize Brownian motion from undersampled data.

IMAGE PREPROCESSING

During image acquisition there are many factors that may cause image quality degradation, resulting in a corrupted representation of reality. First of all, as explained in the previous section, illumination levels must often be kept to a minimum to avoid photobleaching and photodamage, especially in fluorescence microscopy. As a consequence, the SNR in the resulting images is usually very low. Second, any optical imaging device has limited resolution, due to the diffraction phenomenon, which manifests itself as blurring in the acquired images. Third, especially in widefield microscopy imaging, out-of-focus light also contributes to the image, causing a loss of contrast for in-focus objects and contributing to the perception of a blurred image. Finally, even if the microscope setup is perfectly stable, unwanted motion may occur in the specimen. This is the case, for example, when studying intracellular dynamic processes while the cells themselves are migrating. In this section we briefly discuss methods developed specifically for reducing these artifacts. A more in-depth discussion of these methods can be found elsewhere in this volume or in other works [100].

Image Denoising

Any image acquired with a physical device will be contaminated with noise. While different uses of the word exist, in the context of this chapter we refer to noise as any random fluctuation in image intensity, as opposed to systematic distortions, such as hot or cold pixels in charge-coupled devices (CCDs), or background shading phenomena, which can be compensated for. In optical microscopy imaging, noise originates from a variety of sources, which may be subdivided into four categories: 1) the quantum nature of light, which gives rise to photon noise, 2) random electron generation due to thermal vibrations, called thermal noise, 3) random fluctuations in the analog electric signals in the imaging sensors before digitization, referred to as readout noise, and 4) round-off errors introduced by converting the analog signal to a digital one, known as quantization noise. Whereas thermal, readout, and quantization noise can be made negligible by proper electronic design and careful operating conditions, photon noise (also called shot noise) is inherent to optical imaging and constitutes the limiting source of random image intensity fluctuation [149,125].

Although noise cannot be avoided during acquisition, it can be reduced afterwards to some degree by image processing. A wide variety of so-called denoising methods are available for this purpose, which can be divided into linear versus nonlinear filtering methods. The former consist in linearly weighing and summing input values in a signal-independent fashion to produce the output values. Examples of this are uniform local averaging [54] and Gaussian smoothing [151]. While effective in reducing noise, these methods also blur relevant image structures. To avoid this effect, the blurring must be made signal-dependent, which can be accomplished by using nonlinear methods. The most commonly used example of this is median filtering [50,16,114]. More sophisticated methods that are increasingly being used also in time-lapse imaging [3,50,145,117,143] are based on the principle of anisotropic diffusion filtering [101] or wavelet-based denoising [31]. Avoiding blurring near object edges, these methods usually yield superior results. To remove not only noise but also small-scale image structures, methods based on gray-level morphology [121] have also been used successfully [1,3].

Image Deconvolution

Conventional widefield microscopes are designed to image specimens at the focal plane of the objective lens, but they also collect light emanating from off-focus planes, causing reduced contrast of in-focus image structures. In confocal microscopes, this off-focus light is largely rejected by the use of pinholes, resulting in clearer images and increased resolution, both laterally and axially [100]. In either case, however, diffraction occurs as the light passes through the finite-aperture optics of the microscope, introducing a blurring effect. For a well designed imaging system, this blurring can be accurately modeled mathematically as a convolution of the true incident light distribution with the point spread function (PSF) of the system [160,18]. If the PSF is known, it is in principle possible to reverse this operation, at least partially. This is called deconvolution.

A number of methods are available for deconvolution, which vary greatly in computational demand, the requirement to have accurate knowledge of the PSF, and their ability to not only reduce blur, improve contrast, and increase resolution, but also to suppress noise [116,18,62]. Similar to denoising methods, they can be divided into linear versus nonlinear methods. The former category includes the nearest-neighbor and Fourier-based inverse filtering algorithms, which are conceptually simple and computationally fast, but have the tendency to amplify noise and even introduce artifacts. Generally they are not recommended, especially when studying small, intracellular structures and dynamic processes. More sophisticated, nonlinear methods involve iterative constrained algorithms, which better allow enforcing specific behavior. The latter category also includes so-called blind deconvolution algorithms [62], which in contrast with other algorithms do not require knowledge of the PSF, as it is estimated from the data in the process. Time-lapse imaging of thick samples, such as tissue, may require even more sophisticated, space-variant deconvolution methods [67].

While some authors have advocated to always deconvolve all image data if possible [18], the question whether deconvolution, as a separate preprocessing step, is really necessary or beneficial depends on the application. Particularly in studies requiring tracking of subresolution particles, explicit deconvolution seems less relevant, except perhaps when widefield microscopes are used [49,78]. This is because the localization of such particles, which appear in the images as diffraction-limited spots, can be done with much higher accuracy and precision than the resolution of the imaging system [105,2,108,138]. Especially when the detection and localization algorithm involves fitting (a model) of the PSF, to some degree this is in fact deconvolution, carried out implicitly in the process. This probably explains why most reports on particle tracking do not mention the use of deconvolution.

Image Registration

One of the difficulties frequently encountered in quantitative motion analysis is the presence of unwanted movements confounding the movements of interest. Especially in time-lapse imaging of living specimen, the movements of the structures of interest are often a superposition of global displacements and deformations of the specimen and the true local movements [49,50]. For example, in intravital microscopy studies, which involve living animals, the image sequences may show cardiac, respiratory, or other types of global motion artifacts [40,53,118]. But even in the case of imaging live cell cultures, the dynamics of intracellular structures may be obscured by cell migration, deformation, or division [9,16,112,115]. In such situations, prior motion correction is necessary, which can be achieved by global or local image alignment, also referred to as image registration.

Many image registration methods have been developed over the past decade, for a wide variety of applications, notably in clinical medical imaging [61,56,85,102]. The most important aspects of a registration method, which determine its suitability for a specific registration problem, are the type of in-

formation (extrinsic or intrinsic) and the measure (such as cross-correlation or mutual information) used to quantify the similarity of images, the type of geometrical transformations supported (rigid, that is translation and rotation, versus non-rigid, which also includes scaling and affine or even elastic deformations), and various implementational issues (such as the interpolation, optimization, and discretization strategies used). From the large body of literature on the subject, it was recently concluded [102] that the currently popular mutual-information based methods are suitable for numerous clinical applications, but that they may not be the universal cure for all registration problems. Also, specific implementation choices may have a large influence on the results.

In biological imaging, image registration methods are not as abundant as in clinical medical imaging, although they are increasingly used in time-lapse microscopy imaging applications. The methods published to date vary greatly in implementation and application. For the tracking of leukocytes in phase-contrast images, for example, normalized cross correlation of edge information was successfully used to achieve translational background registration [1,40,53]. By contrast, tracking of intracellular particles in fluorescence microscopy image sequences usually requires correction for translation as well as rotation or even more complex deformations of cells or nuclei, by intensity-based cross correlation [16] or by using the labeled proteins as landmarks in an (iterative) point-based registration scheme [17,112,48]. Since, in the case of fluorescence microscopy, large parts of the images often bear no relevant information, the use of landmarks can indeed be expected to improve the robustness and accuracy of registration [30,131]. However, due to a lack of extensive experimentation with different approaches, there is at present no clear consensus about which method works best.

IMAGE ANALYSIS

The ultimate goal of time-lapse imaging experiments is to gain insight into (intra)cellular dynamic processes. Inevitably this requires quantitative analysis of motion patterns. Basically there are three categories of approaches to this problem. The first consists of real-time, single-target tracking techniques. These usually involve a microscope setup containing an image based feedback loop controlling the positioning and focusing of the system to keep the object of interest in the center of the field of view [5,12,14,75,106,107,126]. Only a small portion of the specimen is illuminated this way, which reduces photodamage and allows faster and/or longer imaging. The second category consists of ensemble tracking approaches, such as fluorescence recovery after photobleaching (FRAP), or loss in photobleaching (FLIP) [80,133]. While powerful in assessing specific dynamics parameters, such as diffusion coefficients and association/dissociation rates, they are limited to yielding averages over larger populations. The third category, on which we focus here, consists of approaches that aim to track all individual objects of interest present in the data, and are usually performed off-line.

As pointed out in the introduction of this chapter, the huge amounts of image data generated by time-lapse experiments nowadays call for computerized image analysis. Different levels of computerization exist, ranging from simply facilitating image browsing and manual analysis [19,58,63,137], to manual initialization followed by automated tracking, to full automation (cf. Tables 1 and 2). In the interest of time efficiency, objectivity, and reproducibility, the latter is to be preferred. However, due to the large variety of microscopy imaging techniques and cellular components of interest, the objects to be tracked may have widely differing or even time-varying appearances in the images. As a consequence, full automation can usually be achieved only by developing very dedicated algorithms. This explains the large body of literature on the subject. It also explains why existing commercial tracking software tools, which, understandably, are developed to be as generally applicable as possible, often fail to yield satisfactory results for specific tracking tasks.

In this section we discuss published approaches to automated object tracking in time-lapse microscopy images. A distinction is made between cell tracking and particle tracking. Two different strategies exist for both problems. The first consists in the identification of the objects of interest in the entire image sequence, separately for each frame, followed by temporal association, which tries to relate identified objects either globally over the entire sequence or from frame to frame. In the second strategy, objects of interest are identified only in a first frame, and are subsequently followed in time by matching or model evolution. In either case, the algorithms usually include a detection or segmentation stage, and a temporal association stage. Both are essential in order to be able to perform motion analysis of individual objects. Alternative approaches, based on optic flow, have also been studied [144,11,50,51,94, 127], but these are limited to computing collective cell motion and intracellular particle flows, unless additional detection algorithms are applied.

Cell Tracking

Cell motility and migration are of fundamental importance to many biological processes [24,34,45,129, 152,166]. In embryonic development, for example, cells migrate and differentiate into specific cell types to shape different organs. Failures in this process may result in severe congenital defects and diseases. But also in adult organisms, cell movement continues to play a crucial role. In wound healing, several interrelated cell migration processes are essential in regenerating damaged tissue. The immune system consists of many different proteins and cells interacting in a dynamic network to identify and destroy infectious agents. Many disease processes, most notably cancer metastasis, depend heavily on the ability of cells to migrate through tissue and reach the blood stream. It is because of its importance for basic cell biology as well as its medical implications that cell migration is a very active field of research. Automated methods for segmenting and following cells over time (Table 1) are becoming essential in quantifying cell movement and interaction under normal and perturbed conditions.

Cell Segmentation

The simplest approach to separate cells from the background is to apply intensity thresholding. This involves only a single parameter, which can be set manually or derived automatically from the data, based on the intensity histogram. While used in many cell tracking algorithms [29,44,76,82,84,87,139, 162], this approach will be successful only if cells are well separated and their intensity levels differ markedly and consistently from the background. In practice, however, this condition is often not met. In phase-contrast microscopy, for example, cells may appear as dark regions surrounded by a bright halo, or vice versa, depending on their position relative to the focal plane. In the case of fluorescence microscopy, image intensity may fall as a function of time due to photobleaching. While the situation may be improved by using adaptive thresholding or some sort of texture filtering [8,32,130,157], thresholding based on image intensity alone is generally not recommended.

A fundamentally different approach to cell detection and segmentation that is particularly relevant to phase-contrast or differential interference contrast microscopy, is to use a predefined cell intensity profile, also referred to as a template, to be matched to the image data. This works well for cells that do not change shape significantly, such as certain blood cells or algal cells [66,161]. However, most cell types are highly plastic and move by actively changing shape. Keeping track of such morphodynamic changes would require the use of a large number of different templates, which is impractical from the point of view of both algorithm design and computational demands.

Another well-known approach to image segmentation is to apply a so-called watershed transform [148,55]. By considering the image as a topographic relief and by flooding this relief from the local minima, this transform completely subdivides the image into regions and delimiting contours, which,

by analogy, are termed catchment basins and watersheds, respectively. This is a simple yet intuitively sensible method for which fast implementations exist that can easily be parallelized. The basic algorithm has several notorious drawbacks, however, such as sensitivity to noise and the tendency to yield oversegmentation [55], which call for carefully designed pre- and postprocessing strategies in order to achieve acceptable results. By using marking, gradient-weighted distance transformation, and model-based merging methods, several authors have successfully applied the watershed transform to cell segmentation in microscopy [3,57,79,86,151,159].

Currently there is an increasing interest in the use of deformable models for cell segmentation [27,33, 37,69,96,109,111,117,124,164,165,166]. These are closed fronts, usually parametric active contours or "snakes" [68] in 2D and implicit active surfaces or level sets [122] in 3D, which iteratively evolve in the image domain to optimize a predefined energy functional. Typically this functional consists of both image-related terms and image-independent terms. The former may contain statistical measures of intensity and texture in the region enclosed by the front, or gradient magnitude information along the front. Image-independent terms concern properties of the shape itself represented by the front, such as boundary length or surface area, curvature, and the similarity to reference shapes. It is this mixture of terms, which enables flexible incorporation of both image information and prior knowledge, that makes deformable models easily adaptable to specific applications [37,166].

Cell Association

Several strategies exist to perform interframe cell association. The simplest is to associate each segmented cell in one frame with the nearest cell in a subsequent frame, where "nearest" may not only refer to spatial distance [25,29,32,36,70,82,87], for example between boundary points or centroid positions, but also to similarity in terms of average intensity, area or volume, perimeter or surface area, major and minor axes orientation, boundary curvature, angle or velocity smoothness, and other features [23,40,44,76,83]. Generally, the more features, the lower the risk of ambiguity. However, matching a large number of features may be similarly restricting as template matching [1,8,71,155], as cell shape changes between frames can be less easily accommodated. Some applications, on the other hand, may not require keeping track of cell shape features, and in such cases robust tracking of just cell center position may be achieved by (coupled) mean-shift processes [28,159].

The increasing interest in deformable model approaches, mentioned above, can be attributed not only to their flexibility in performing cell segmentation. By construction, they also lend themselves naturally to capturing both cell migration and cell shape changes over time [166]. At any time, the contours or surfaces obtained in the previous frame of an image sequence can be used as initialization for the segmentation process in the current frame [37,77,96,164]. When using standard algorithms, however, this usually works well only if cell displacements are limited to at most one cell diameter from frame to frame [37,109]. Otherwise, more sophistication is required, such as the use of gradient-vector flows [111,109,158,164] or the incorporation of known or estimated dynamics [27,124].

Concerning the choice of explicitly defined models (parametric active contours) versus implicitly defined models (through level sets), recent research efforts have shown a preference towards the latter, since they can easily handle topological changes, such as cell division, and can readily be extended to deal with higher-dimensional image data [37]. In either case, however, several adaptations to the standard algorithms are usually necessary to be able to simultaneously track multiple cells and to properly handle cell contacts, appearances, and disappearances. While this is certainly feasible [37,96,111, 164], it usually introduces a number of additional parameters that must be tuned empirically for each specific application, which potentially increases the risk of errors and reduces reproducibility. In turn, this may require postprocessing steps to validate tracking results [110].

Particle Tracking

The ability of cells to migrate, perform a variety of specialized functions, and to reproduce, is the result of a large number of intracellular processes involving thousands of differently sized biomolecular complexes, collectively termed "particles" in this chapter. Since many diseases originate from a disturbance or failure of one or more of these processes, they constitute the subject of intense current research, by academic institutes as well as pharmaceutical companies. Visualization of intracellular particles has become possible only relatively recently, with the advent of fluorescent probes [81,95]. Combined with time-lapse optical microscopy imaging they enable studying the dynamics of virtually any protein in living cells. Automated image analysis methods for detecting and following fluorescently labeled particles over time (Table 2) are becoming indispensable in order to take full advantage of the image data acquired for such studies [93].

Particle Detection

In fluorescence microscopy imaging, the particles of interest are never observed directly, but their position is revealed indirectly by the fluorescent molecules attached to them. Typically these fluorophores are cylindrically shaped molecules having a length and diameter on the order of a few nanometers only. In most experimental cases it is unknown how many fluorescent molecules are actually attached to the particles of interest. Commonly, however, a fluorescently labeled particle will be much smaller than the optical resolution of the imaging system. Even though recent advances in light microscopy have opened the way to imaging with significantly improved resolution [13,38,59,60,113], the resolution of most confocal microscopes currently in use today is limited to around 200 nm in-plane and around 600 nm axially. Therefore, fluorescently labeled particles effectively act as point light sources, and consequently they appear in the images as diffraction-limited spots, also called foci.

The question to what accuracy single particles can be localized, and to what extent multiple particles can be resolved, has been the subject of several recent studies [2,98,105,108,138]. From these studies it follows that localization accuracy and resolvability depend on a number of factors. If magnification and spatial sampling are properly matched to satisfy the Nyquist criterion, the limiting factor is the SNR, or effectively the photon count, with higher photon counts yielding higher accuracy and resolvability. The consensus emerging from these studies seems to be that for single particles, a localization accuracy of around 10 nm is achievable in practice. Estimation of the distance between two particles is possible with reasonable levels of accuracy for distances of about 50 nm and larger. Smaller distances can be resolved but with rapidly decreasing accuracy. In order to improve accuracy in such cases, the number of detected photons would have to be increased substantially, which is typically not possible in time-lapse imaging experiments without causing excessive photobleaching.

A number of approaches to particle detection and localization exist. Similar to cell segmentation, the simplest approach to discriminate between objects and background is to apply intensity thresholding. The localization of a particle is often accomplished by computing the local centroid, or center of intensity, of image elements with intensity values above a certain threshold [6,16,52,78,83,103,156]. Clearly, such threshold-based detection and localization will be successful only in cases of no or very limited photobleaching, unless some form of time-adaptive thresholding is applied. More robustness can be expected from using the intensity profile of an imaged particle in one frame in a template matching process to detect the same particle in subsequent frames [46,135]. This approach can be taken one step further by using a fixed template representing the theoretical profile of a particle. In the case of diffraction-limited particles, this profile is in fact the PSF of the microscope, which in practice is often approximated by the Gaussian function [4,72,73,163]. Extensions of this approach involving

Gaussian mixture model fitting for detecting multiple, closely positioned particles simultaneously have also been reported [35,136]. For larger particles with varying shapes and sizes, detection schemes using wavelet-based multiscale products have been successfully applied [47,99].

In a recent study [22], several common algorithms for particle detection/localization were quantitatively compared as a function of SNR and object diameter, in terms of both accuracy (determinate errors or bias) and precision (indeterminate errors). The algorithms included two threshold-based centroid detection schemes, Gaussian fitting, and template matching using normalized cross-correlation or the sum of absolute differences as similarity measures. It was concluded that for particles with diameter less than the wavelength, Gaussian fitting is the best approach by several criteria. For particles having much larger diameter, cross-correlation based template matching appears to be the best choice. It was also concluded that the SNR constitutes the limiting factor of algorithm performance. As a rule of thumb, the SNR should be at least 5 in order to achieve satisfactory results using these algorithms. Subsequent evaluation studies [20] even mentioned SNR values of 10 and higher. Since such levels are quite optimistic in practice, especially in time-lapse imaging experiments, the quest for more robust detection schemes is likely to remain for some time to come.

Particle Association

Similar to cell association, the simplest approach to particle association is to use a nearest-neighbor criterion, based on spatial distance only [6,52,54,73,78,88]. While this may work well in sparse specimen, containing very limited numbers of well spaced particles, it will fail to yield unambiguous results in cases of higher particle densities. In order to establish the identity of particles from frame to frame in such cases, additional cues are necessary. When tracking subresolution particles, for example, the identification may be improved by taking into account intensity and spatiotemporal features such as velocity and acceleration, as estimated from previous frames [4,9,120]. Larger particles may also be distinguished by using spatial features such as size, shape, or orientation [156]. In the limit, matching a large number of spatial features is similar to performing template matching [16,35].

Rather than finding the optimal match for each particle on a frame-by-frame basis, the temporal association problem may also be solved in a more global fashion. Such an approach is especially favorable in more complex situations of incomplete or ambiguous data. For example, particles may temporarily disappear, because they move out of focus for some time, or, as in the case of quantum dots, the fluorescence of the probe is intermittent. In the case of single particles, or limited numbers of well-spaced particles, this problem has been solved by translating the tracking task into a spatio-temporal segmentation task and finding optimal paths through the entire data [15,115].

The problem becomes more complicated, however, in the case of high particle densities and the possibility of particle interaction. For example, two or more subresolution particles may pass or approach each other so closely at some point in time that they appear as a single spot that cannot be dissolved by any detector, and they may separate at some later time to form multiple spots again. Keeping track of all particles in such cases requires some form of simultaneous association and optimization. Several authors [120,135,136,146] have proposed to solve the problem using graph-theoretic approaches, in which the detected particles and all possible correspondences and their likelihoods together constitute a weighted graph, and the subgraph representing the best overall solution is obtained by applying a global optimization algorithm.

Most particle tracking algorithms published to date are deterministic, in the sense that they make hard decisions about the presence or absence of particles in each image frame, and the correspondence of

particles between frames. There is now an increasing interest in the use of probabilistic approaches [47,128] to reflect the uncertainty in the image data. Typically, these approaches consist of a Bayesian filtering framework, and involve models of object dynamics, to be matched to the data. It has been argued that incorporating assumptions about the kinematics of object motion is risky in biological tracking, as little is known about the laws governing the motion, and the purpose of tracking is to deduce this [8]. However, biological investigation is an iterative endeavor, leading to ever refined models of cellular and molecular structure and function, and it makes sense at each iteration to take advantage of the knowledge acquired in previous iterations.

TRAJECTORY ANALYSIS

The final stage in any time-lapse microscopy imaging experiment is the analysis of the trajectories resulting from cell or particle tracking, to confirm or reject predefined hypotheses about object dynamics, or to discover new phenomena. Qualitative analysis by visual inspection of computed trajectories may already give hints about trends in the data, but usually does not provide much more information than can be obtained by directly looking at the image data itself, or projections thereof. Quantitative analyses of the trajectories are required in order to achieve higher sensitivity in data interpretation and to be able to perform statistical tests. Of course, what parameters to measure and analyze depends very much on the research questions underlying a specific experiment. Here we briefly discuss examples of measurements frequently encountered in the literature.

Geometry Measurements

Once the objects of interest in an image sequence are detected, segmented, and associated, a multitude of measures concerning the geometry of the resulting trajectories as well as the objects themselves can readily be computed. An example is the maximum relative distance to the initial position reached by the object [27,28,57]. Other examples are the length of the trajectory, or the total distance traveled by the object, and the distance between start and end point, or the net distance traveled [12]. The latter measures relate to the so-called McCutcheon index [32,91], which is often used in chemotaxis studies to quantify the efficiency of cell movements, and is defined as the ratio between the net distance moved in the direction of increasing chemoattractant concentration and the total distance moved. Derived parameters, such as the directional change per time interval and its autocorrelation [129,154], are indicative of the directional persistence and memory of a translocating cell. Information about the cell contour or surface at each time point allow the computation of a variety of shape features, such as diameter, perimeter and area, or surface area and volume, circularity or sphericity, convexity or concavity [129], elongation or dispersion [33], and their changes over time.

Diffusivity Measurements

A very frequently studied parameter, especially in particle tracking experiments, is the mean square displacement (MSD) [4,6,16,35,54,72,74,78,89,115]. It is a convenient measure to study the diffusion characteristics of the motion of individual particles [104,119,134] and also allows to assess the viscoelastic properties of the media in which they move [140,141,134]. By definition, the MSD is a function of time lag, and the shape of the MSD-time curve for a given trajectory is indicative of the mode of motion of the corresponding particle (Figure 4). For example, in the case of pure or normal diffusion by thermally driven Brownian motion, the MSD will increase linearly as a function of time, where the diffusion constant determines the slope of the line. In the case of flow or active transport, on the other hand, the MSD will increase more rapidly and in a nonlinear fashion. The contrary case of anomalous subdiffusion, characterized by a lagging MSD-time curve compared to normal diffusion, occurs if the motion is not free but impeded by obstacles. Confined motion, caused by corrals or tethering or other

restrictions, manifests itself by a converging curve, where the limiting MSD value is proportional to the size of the region accessible for diffusion. Mathematically, the MSD is the second-order moment of displacement. A more complete characterization of a diffusion process is obtained by computing all moments of displacement up to some order [43,120].

Some prudence is called for in diffusivity measurements. In isotropic media, where the displacements in each of the three spatial dimensions may be assumed to be uncorrelated, the 2D diffusion coefficient is equal to the 3D diffusion coefficient [134]. In practical situations, however, it may be unknown a priori whether isotropy can be assumed. In this context we recall our warning remarks regarding 2D versus 3D motion analysis [35,152,166] and stress again the importance of experimental verification of one's assumptions. Furthermore, the diffusivity of a particle may depend on the diameter of the particle compared to the microstructure of the biological fluid in which it moves. Here, a distinction must be made between microscopic, mesoscopic, and macroscopic diffusion [134]. Also, in the case of normal diffusion, the relation between the slope of the MSD-time line and the diffusion constant strictly holds only for infinite trajectories [104]. The shorter the trajectories, the larger the statistical fluctuations in the diffusivity measurements, and the higher the relevance of studying distributions of diffusion constants rather than single values. But even for very long trajectories, apparent subdiffusion patterns may arise at short time scales, caused solely by the uncertainty in particle localization in noisy images [89]. Finally, care must be taken in computing the MSD over an entire trajectory, as it may obscure transitions between diffusive and nondiffusive parts [119].

Velocity Measurements

Another commonly studied parameter in time-lapse imaging experiments is velocity [10,29,32,57,90, 127,153]. It is computed simply as distance over time. Instantaneous object velocity can be estimated as the distance traveled from one frame to the next divided by the time interval. Average velocity, also referred to as curvilinear velocity, is then computed as the sum of the frame-to-frame distances traveled, divided by the total time elapsed. If the temporal sampling rate is constant, this is the same as averaging the instantaneous velocities. The so-called straight-line velocity, another type of average velocity, is computed as the distance between the first and last trajectory position divided by the total elapsed time. The ratio between the latter and the former, known as the linearity of forward progression [70,84,162], is reminiscent of the McCutcheon index mentioned above. Histograms of velocity [10,32, 88,104,144,145,146] are often helpful in gaining insight into motion statistics. Object acceleration can also be estimated from velocity but is rarely studied [129].

Several warning remarks are in order regarding velocity estimation. In the case of cell tracking, motion analysis is tricky, due to the possibility of morphological changes over time. Often, to circumvent the problem, a center position is tracked [25,29,45,63,70,83,84,153,162]. In the case of highly plastic cells, however, centroid based velocity measurements can be very deceptive [129]. For example, an anchored cell may extend and retract pseudopods, thereby continuously changing its centroid position and generating significant centroid velocity, while the cell is not actually translocating. In the contrary case, a cell may spread in all directions at high velocity in response to some stimulant, while the cell centroid position remains unchanged. Another warning concerns the accuracy of velocity estimation in relation to the temporal sampling rate [129]. The higher this rate, the more detailed the movements are captured, and the closer the velocity estimates will approach the true values. Statistically speaking, as the sampling rate decreases, velocities will on average be increasingly underestimated.

SAMPLE ALGORITHMS

In the previous section we have drawn a fairly complete but perhaps somewhat superficial picture of existing methodologies for cell and particle tracking. Space limitations do not permit us to provide a detailed discussion of the pros and cons of all of these methods for different applications. Nevertheless, in order to better appreciate the intricacies of the tracking problem and some of the solutions that have been proposed, we now describe two specific algorithms in more detail, one for cell tracking and one for particle tracking applications. Rather than presenting relatively simple algorithms, which may be easy to understand and implement, but which are likely to show poor performance in practice, we have chosen to briefly describe the main steps of the currently most promising but necessarily more involved cell and particle tracking algorithms. Both are based on the use of models.

Cell Tracking

Possibly the most extensively studied approach to image segmentation in recent years is the use of level-set methods [122]. These methods have also been explored for cell segmentation and tracking [37,39,96], with promising initial results. In contrast with most classical model-based approaches, which involve cumbersome explicit representations of objects by marker points and parametric contours or surfaces [68,92], these methods conveniently define object boundaries in an implicit way as the zero-level set of a scalar function, denoted by $\varphi(.)$ here. This level-set function is defined such that $\varphi(\mathbf{x}) > 0$ when $\mathbf{x}$ lies inside the object, $\varphi(\mathbf{x}) < 0$ when $\mathbf{x}$ is outside the object, and $\varphi(\mathbf{x}) = 0$ at the object boundary, where $\mathbf{x}$ denotes position within the image domain. The important advantages of this representation over explicit representations are its topological flexibility and its ability to handle data of any dimensionality without the need for dedicated modifications.

The idea of level-set based image segmentation is to iteratively evolve the level-set function $\varphi(.)$ so as to minimize a predefined energy functional. In principle, it is possible to define $\varphi(.)$ in such a way that its zero-level includes the boundaries of all objects of interest in the image, and to evolve these boundaries concurrently by evolving this single function. However, in order to have better control over the interaction between object boundaries when segmenting multiple cells, and to conveniently keep track of individual cells, it is advisable to define a separate level-set function, $\varphi_i(.)$, for each object, $i = 1,\ldots,N$. Using this approach, we can define the energy functional as, for example:

$$E(\varphi_1,\ldots,\varphi_N) = \int_\Omega \sum_{i=1}^{N} \Big[\alpha\delta(\varphi_i(\mathbf{x}))\,|\nabla\varphi_i(\mathbf{x})| + H(\varphi_i(\mathbf{x}))e_i(\mathbf{x}) + e_0(\mathbf{x})\frac{1}{N}\prod_{j=1}^{N}(1-H(\varphi_j(\mathbf{x}))) + \gamma\sum_{i<j}H(\varphi_i(\mathbf{x}))H(\varphi_j(\mathbf{x}))\Big]d\mathbf{x} \quad (1)$$

where $\delta(.)$ is the (regularized) Dirac delta function, $H(.)$ denotes the (regularized) Heaviside step function, α and γ are positive parameters, the integral is over the entire image domain, denoted by Ω, and the $e_i(.)$ are object energy functions, with $e_0(.)$ denoting the background energy function. The model-based aspect of the level-set approach lies primarily in the latter functions.

The core of this equation consists of four terms, with intuitive meaning: the first, with weight α, boils down to the magnitude of the object boundary (contour length in 2D and surface area in 3D), the second term adds energy values for positions inside the boundary, the third is the total background energy, and the fourth, with weight γ, is a penalty term for overlapping boundaries. The formula for iterative evolution of the level-set functions corresponding to the N objects follows from the Euler-Lagrange equations associated with the minimization of the functional (1):

$$\partial\varphi_i(\mathbf{x}) = \delta(\varphi_i(\mathbf{x}))\Big[\alpha\nabla\cdot\frac{\nabla\varphi_i(\mathbf{x})}{|\nabla\varphi_i(\mathbf{x})|} - e_i(\mathbf{x}) + e_0(\mathbf{x})\prod_{j\neq i}(1-H(\varphi_j(\mathbf{x}))) - \gamma\sum_{j\neq i}H(\varphi_j(\mathbf{x}))\Big]\partial\tau \qquad (2)$$

where $\partial\tau$ denotes the step size in artificial (evolution) time; that is, for segmentation of a single image frame [21], not to be confused with the real time interval between image frames. Once the energy functional is minimized, and thus a segmentation has been obtained for a given image frame, the resulting level-set functions can be used to compute any morphological feature of interest, and can also serve as initialization for the minimization procedure for the next image frame.

In summary, the main steps of a level-set based tracking algorithm, and the associated points of attention concerning its application to multiple cell tracking in time-lapse microscopy, are:

1. Define the object and background energy functions, $e_i(.)$ and $e_0(.)$, respectively. These functions mathematically describe the deviation of object and background features from their desired values. This allows one to incorporate prior knowledge about cell and background appearance. In practice, it often suffices to model appearance in terms of simple image statistics, such as the deviation from the mean intensity within the cell or background, and intensity variance.

2. Specify the parameters α and γ. These determine the influence of the boundary magnitude and overlap penalty terms, respectively, relative to the object and background energy terms in the total energy functional (1), and are necessarily application dependent. Optimal values for these parameters will have to be obtained by experimentation.

3. Segment the first image of the sequence. This is done by defining a single level-set function $\varphi(.)$ and evolving it according to the single-object version of (2) until convergence. Since proper initialization is crucial to achieve fast convergence and to arrive at the global optimum, the initial level-set function must be chosen as close as possible to the true boundaries. For example, one could apply a simple segmentation scheme, and initialize $\varphi(.)$ based on the outcome.

4. Initialize the level-set functions in the first image of the sequence. Cell objects are obtained by finding connected components in the segmentation resulting from step 3. For each detected object O_i, a level-set function $\varphi_i(.)$ is computed from the signed distance function applied to the boundaries of O_i, with positive values inside and negative values outside O_i.

5. Evolve the level-set functions $\varphi_i(.)$ concurrently according to (2) until convergence. The time step $\partial\tau > 0$ in the discretized version of the evolution equation should be chosen with care. Too small values may cause unnecessarily slow convergence. Conversely, too large values may cause object boundaries to be missed. In practice, values between 0.01 and 0.1 give satisfactory results. To speed up the computations, one could choose to update the level-set functions only for positions $\mathbf{x}$ in a narrow band around the current zero-level sets, for which $\varphi_i(\mathbf{x}) = 0$.

6. Detect incoming and dividing cells. An additional level-set function could be used to detect cells that enter the field-of-view from the boundaries of the image. Cell division could be detected by monitoring cell shape over time. Drastic morphological changes are indicative of approaching division. If, just after such an event, a level-set function contains two disconnected components, one could decide to replace the function by two new level-set functions.

7. Initialize the level-set functions for the next frame of the sequence. This can be done simply by taking the functions from the previous frame. Notice that in order for this approach to work, in practice, cells should not move more than their diameter from frame to frame. To prevent the level-set functions from becoming too flat, in some cases it may be advantageous to reinitialize them to the signed distance to their zero-level after a fixed number of iterations.

8. Repeat steps 5-7 until all frames of the image sequence are processed. The resulting level-set functions $\varphi_t(.)$ as a function of real time enable estimation of the position and morphology of the corresponding cells for each frame in the sequence.

Sample results with specific implementations of this algorithm [37,39] applied to the tracking of the nuclei of proliferating HeLa and Madin-Darby canine kidney (MDCK) cells are shown in Figure 5.

Particle Tracking

An interesting and promising approach to particle tracking that we have recently been experimenting with [47,128] is to cast the temporal association problem into a Bayesian estimation problem. In general, Bayesian tracking deals with the problem of inferring knowledge about the true state of a dynamic system, based on a sequence of noisy measurements, or observations. The state vector, denoted by $\mathbf{x}_t$, contains all relevant information about the system at any (real) time t, such as position, velocity, acceleration, intensity, and shape features. Bayesian filtering consists in recursive estimation of the time-evolving posterior probability distribution $p(\mathbf{x}_t|\mathbf{z}_{1:t})$ of the state $\mathbf{x}_t$, given all measurements up to time t, denoted as $\mathbf{z}_{1:t}$. Starting with an initial prior distribution, $p(\mathbf{x}_0|\mathbf{z}_0)$, with $\mathbf{z}_0 = \mathbf{z}_{1:0}$ being the set of no measurements, the filtering first predicts the distribution at the next time step:

$$p(\mathbf{x}_t|\mathbf{z}_{1:t-1}) = \int D(\mathbf{x}_t|\mathbf{x}_{t-1})\, p(\mathbf{x}_{t-1}|\mathbf{z}_{1:t-1}) d\mathbf{x}_{t-1} \tag{3}$$

based on a Markovian model, $D(\mathbf{x}_t|\mathbf{x}_{t-1})$, for the evolution of the state from time t–1 to time t. Next, it updates the posterior distribution of the current state by applying Bayes' rule:

$$p(\mathbf{x}_t|\mathbf{z}_{1:t}) \propto L(\mathbf{z}_t|\mathbf{x}_t)\, p(\mathbf{x}_t|\mathbf{z}_{1:t-1}) \tag{4}$$

using a likelihood, $L(\mathbf{z}_t|\mathbf{x}_t)$, which models the probability of observing $\mathbf{z}_t$ given state $\mathbf{x}_t$. The power of this approach lies not only in the use of explicit dynamics and observation models, but also in the fact that at any time t, all available information up to that time is exploited.

The above recurrence relations are analytically tractable only in a restricted set of cases, such as when dealing with linear dynamic systems and Gaussian noise, for which an optimal solution is provided by the so-called Kalman filter. In most biological imaging applications, where the dynamics and noise can be expected to be nonlinear and non-Gaussian, efficient numerical approximations are needed, which are provided by sequential Monte Carlo (SMC) methods, such as the CONDENSATION algorithm [65]. In that case, the posterior distribution is represented by N_s random state samples and associated weights:

$$p(\mathbf{x}_t|\mathbf{z}_{1:t}) \approx \sum_{i=1}^{N_s} w_t^{(i)} \delta\left(\mathbf{x}_t - \mathbf{x}_t^{(i)}\right) \tag{5}$$

where $\delta(.)$ is the Dirac delta function, and the weights $w_t^{(i)}$ of the state samples $\mathbf{x}_t^{(i)}$ sum to 1. The problem of tracking large numbers of objects using this framework is conveniently solved by representing the filtering distribution by an M-component mixture model [147]:

$$p(\mathbf{x}_t|\mathbf{z}_{1:t}) = \sum_{m=1}^{M} \omega_{m,t}\, p_m(\mathbf{x}_t|\mathbf{z}_{1:t}) \tag{6}$$

where the weights $\omega_{m,t}$ of the components p_m sum to 1, the total number of samples is $N = M\,N_s$, and each sample is augmented with a component label, denoted by $c_t^{(i)}$, with $c_t^{(i)} = m$ if state sample i belongs to mixture component m. This representation is updated in the same fashion as the single-object case. At each time step, statistical inferences about the state, such as the expected value, or the maximum a posteriori (MAP) or minimum mean square error (MMSE) values, can easily be approximated from the weighted state samples for each object.

In summary, the main steps of an SMC-based tracking algorithm, and the associated points of attention concerning its application to multiple particle tracking in time-lapse microscopy, are:

1. Define the state vector $\mathbf{x}_t$. In most experimental situations it will be sufficient to include position (x_t, y_t, z_t), velocity $(v_{x,t}, v_{y,t}, v_{z,t})$, acceleration $(a_{x,t}, a_{y,t}, a_{z,t})$, and intensity (I_t).

2. Define the state evolution model $D(\mathbf{x}_t|\mathbf{x}_{t-1})$. This model mathematically describes the probability of a particle to jump from the previous state $\mathbf{x}_{t-1}$ to state $\mathbf{x}_t$. It allows one to incorporate prior knowledge about the dynamics of the objects to be tracked and is therefore necessarily application dependent. An example of such a model is the Gaussian weighted deviation of $\mathbf{x}_t$ from the expected state at time t based on $\mathbf{x}_{t-1}$ (for instance, expected position at time t based on velocity at time t–1, and expected velocity at t based on acceleration at t–1). This framework also permits the use of multiple interacting models to deal with different types of motion concurrently (such as random walk, or directed movement, with constant or changing velocity). Notice that having I_t as part of the state vector allows one to also model the evolution of particle intensity (photobleaching).

3. Define the observation model $L(\mathbf{z}_t|\mathbf{x}_t)$. This model mathematically describes the likelihood or probability of measuring state $\mathbf{z}_t$ from the data, given the true state $\mathbf{x}_t$. It allows one to incorporate knowledge about the imaging system, in particular the PSF, as well as additional, static object information, such as morphology. Such a model could, for example, be defined as the Gaussian weighted deviation of the total measured intensity in a neighborhood around $\mathbf{x}_t$, from the expected total intensity based on a shape model of the imaged objects, and from the background intensity, taking into account the noise levels in the object and the background.

4. Specify the prior state distribution $p(\mathbf{x}_0|\mathbf{z}_0)$. This can be based on information available in the first frame. For example, one could apply a suitable detection scheme to localize the most prominent particles, and for each detected particle add a Gaussian shaped mixture component p_m with weight $\omega_{m,0}$ proportional to size or intensity. Each component is then sampled N_s times to obtain state samples $\mathbf{x}_t^{(i)}$ and associated weights $w_t^{(i)}$ for that component. The detection step does not need to be very accurate: false positives will rapidly be filtered out as the system evolves.

5. Use the posterior state distribution $p(\mathbf{x}_{t-1}|\mathbf{z}_{1:t-1})$ at time t–1 to compute the predicted state distribution $p(\mathbf{x}_t|\mathbf{z}_{1:t-1})$ at time t according to (3), and subsequently use this prediction to compute the updated posterior state distribution $p(\mathbf{x}_t|\mathbf{z}_{1:t})$ according to (4). Effectively this is done by inserting

each sample $\mathbf{x}_{t-1}^{(i)}$, $i = 1,\ldots,N$, into the state evolution model, taking a new sample from the resulting probability density function to obtain $\mathbf{x}_t^{(i)}$, and computing the associated weight $w_t^{(i)}$ from $w_{t-1}^{(i)}$ based on the likelihood and dynamics models and an auxiliary importance function. A penalty function can be used to regulate particle coincidence.

6. Update the sample component labels $c_t^{(i)}$. This step is necessary if particle merging and splitting events are to be captured. It involves the application of a procedure to recluster the state samples from the M mixture components to yield M' new components. This procedure can be implemented in any convenient way and allows one to incorporate prior knowledge about merging and splitting events. In the simplest case one could apply a K-means clustering algorithm.

7. Update the mixture component set and the corresponding weights $\omega_{m,t}$. To determine whether particles have appeared or disappeared at any time t, one could apply some detection scheme as in step 4 to obtain a particle probability map, and compare this map to the current particle distribution, as follows from the posterior $p(\mathbf{x}_t|\mathbf{z}_{1:t})$. For each appearing particle, a new mixture component is added with predefined initial weight ω_b. Components with weights below some threshold ω_d are assumed to correspond to disappearing particles and are removed from the mixture. The weights $\omega_{m,t}$ are computed from the $\omega_{m,t-1}$ and the weights $w_t^{(i)}$ of the state samples.

8. Repeat steps 5-7 until all frames of the image sequence are processed. The resulting posterior state distributions $p_m(\mathbf{x}_t|\mathbf{z}_{1:t})$ enable estimation of the states of the corresponding particles at any t.

Sample results with a specific implementation of this algorithm [128] applied to the tracking of microtubule plus-ends in the cytoplasm and androgen receptor proteins in the cell nucleus are shown in Figure 6. Experiences with an alternative but related Bayesian filtering algorithm [47] applied to the tracking of cytoplasmic and nuclear HIV-1 complexes can be found in [7].

SUMMARY OF IMPORTANT POINTS

In this chapter we have sketched the current state of the art in time-lapse microscopy imaging, from the perspective of automated image processing and analysis, in particular cell and particle tracking. While it is clear that biological investigation is increasingly relying on computerized methods, it also follows from the plethora of published works discussed here that such methods are still very much in their infancy. Although there is a growing consensus about the strengths and weaknesses of specific approaches, there is currently no single best solution to the problem in general. On the contrary, the main conclusion emerging from the literature is that with currently available image processing and analysis methodologies, any given tracking application requires its own dedicated algorithms to achieve acceptable results. Nevertheless, a number of important points follow from the collective experiences reported to date, and we conclude this chapter by summarizing them. They are listed here in the order in which they follow from the discussions in the main text.

1. Living cells are sensitive to photodamage and require economizing light exposure.
2. Success rates of automated image analysis generally increase with increasing SNR.
3. Time-lapse microscopy involves trading SNR against spatial and temporal resolution.
4. Biological processes occur in 3D+t and should preferably be studied as such.
5. Studies in 2D+t should be accompanied by 3D+t experiments confirming their validity.
6. Sampling theory applies not only to sampling in space but also to sampling in time.
7. Nonlinear filtering methods allow reducing noise while preserving strong gradients.
8. Deconvolution of time-lapse microscopy imaging data is not always necessary.

9. Object motion is often a superposition of global and true local displacements.
10. Correction for global motion can be accomplished by image registration methods.
11. Object tracking requires dedicated detection, segmentation, and association methods.
12. Optic flow methods can be used to compute collective cell motion and particle flows.
13. Image intensity thresholding alone is generally not recommended for segmentation.
14. Template matching works best for objects that do not change shape significantly.
15. Watershed based segmentation requires careful pre- and postprocessing strategies.
16. Deformable models allow easy use of both image information and prior knowledge.
17. By design, deformable models are very suitable for capturing morphodynamics.
18. Implicitly defined models are generally more flexible than explicitly defined models.
19. In fluorescence microscopy, objects are observed only indirectly, via fluorescent probes.
20. Fluorescent (nano)particles act as point light sources and appear as PSF-shaped spots.
21. Particle localization accuracy and resolvability depend strongly on photon count.
22. For single particles, a localization accuracy of around 10 nm is achievable in practice.
23. Two particles are resolvable with reasonable to good accuracy for distances > 50 nm.
24. Gaussian fitting is most suitable for detecting particles with diameter < wavelength.
25. Template matching is most suitable for detecting particles with diameter >> wavelength.
26. For most particle detection methods the SNR must be > 5 to achieve satisfactory results.
27. Reliable temporal association usually requires more criteria than just spatial distance.
28. Tracking of many closely spaced particles requires some form of joint association.
29. Probabilistic tracking methods naturally reflect the uncertainty in the image data.
30. Models of object dynamics are helpful in tracking but should be used with care.
31. Displacement moments provide detailed information about diffusion characteristics.
32. The shape of the MSD-time curve of an object is indicative of the mode of motion.
33. In isotropic media, the 2D diffusion coefficient is equal to the 3D diffusion coefficient.
34. Distinction must be made between microscopic, mesoscopic, and macroscopic diffusion.
35. Short trajectories show large statistical fluctuations in diffusivity measurements.
36. Subdiffusive patterns at short time scales may be due to noise in particle localization.
37. Computing the MSD over entire trajectories may obscure transitions in diffusivity.
38. Different velocity measures result from considering different distance measures.
39. Centroid based velocity measurements can be very deceptive in cell tracking.
40. Velocities will be increasingly underestimated with decreasing temporal resolution.

ACKNOWLEDGMENTS

The authors are grateful to Niels Galjart, Jeroen Essers, Adriaan Houtsmuller, Gert van Cappellen, and Timo ten Hagen of the Erasmus MC, University Medical Center Rotterdam, the Netherlands, for providing the image data used in this chapter for illustrational purposes. Research on tracking methodology in the lab of Erik Meijering is financially supported by the Netherlands Organization for Scientific Research (NWO) through VIDI-grant 639.022.401.

REFERENCES

[1] S. T. Acton, K. Wethmar, K. Ley, "Automatic tracking of rolling leukocytes in vivo," *Microvascular Research* 63(1):139-148, 2002.

[2] F. Aguet, D. Van De Ville, M. Unser, "A maximum-likelihood formalism for sub-resolution axial localization of fluorescent nanoparticles," *Optics Express* 13(26):10503-10522, 2005.

[3] H. Ancin, B. Roysam, T. E. Dufresne, M. M. Chestnut, G. M. Ridder, D. H. Szarowski, J. N. Turner, "Advances in automated 3-D image analysis of cell populations imaged by confocal microscopy," *Cytometry* 25(3):221-234, 1996.

[4] C. M. Anderson, G. N. Georgiou, I. E. G. Morrison, G. V. W. Stevenson, R. J. Cherry, "Tracking of cell surface receptors by fluoresence digital imaging microscopy using a charge-coupled device camera," *Journal of Cell Science* 101(2):415-425, 1992.
[5] S. B. Andersson, "Tracking a single fluorescent molecule with a confocal microscope," *Applied Physics B: Lasers and Optics* 80(7):809-816, 2005.
[6] J. Apgar, Y. Tseng, E. Fedorov, M. B. Herwig, S. C. Almo, D. Wirtz, "Multiple-particle tracking measurements of heterogeneities in solutions of actin filaments and actin bundles," *Biophysical Journal* 79(2):1095-1106, 2000.
[7] N. Arhel, A. Genovesio, K.-A. Kim, S. Miko, E. Perret, J.-C. Olivo-Marin, S. Shorte, P. Charneau, "Quantitative four-dimensional tracking of cytoplasmic and nuclear HIV-1 complexes," *Nature Methods* 3(10):817-824, 2006.
[8] V. Awasthi, K. W. Doolittle, G. Parulkar, J. G. McNally, "Cell tracking using a distributed algorithm for 3-D image segmentation," *Bioimaging* 2(2):98-112, 1994.
[9] C. P. Bacher, M. Reichenzeller, C. Athale, H. Herrmann, R. Eils, "4-D single particle tracking of synthetic and proteinaceous microspheres reveals preferential movement of nuclear particles along chromatin-poor tracks," *BMC Cell Biology* 5(45):1-14, 2004.
[10] A. Bahnson, C. Athanassiou, D. Koebler, L. Qian, T. Shun, D. Shields, H. Yu, H. Wang, J. Goff, T. Cheng, R. Houck, L. Cowsert, "Automated measurement of cell motility and proliferation," *BMC Cell Biology* 6(1):19, 2005.
[11] C. B. J. Bergsma, G. J. Streekstra, A. W. M. Smeulders, E. M. M. Manders, "Velocity estimation of spots in three-dimensional confocal image sequences of living cells," *Cytometry* 43(4):261-272, 2001.
[12] G. S. Berns, M. W. Berns, "Computer-based tracking of living cells," *Experimental Cell Research* 142(1):103-109, 1982.
[13] E. Betzig, G. H. Patterson, R. Sougrat, O. W. Lindwasser, S. Olenych, J. S. Bonifacino, M. W. Davidson, J. Lippincott-Schwartz, H. F. Hess, "Imaging intracellular fluorescent proteins at nanometer resolution," *Science* 313(5793):1642-1645, 2006.
[14] Ph. Bodin, S. Papin, C. Meyer, P. Travo, "Study of living single cells in culture: Automated recognition of cell behavior," *Laboratory Investigation* 59(1):137-143, 1988.
[15] S. Bonneau, M. Dahan, L. D. Cohen, "Single quantum dot tracking based on perceptual grouping using minimal paths in a spatiotemporal volume," *IEEE Transactions on Image Processing* 14(9):1384-1395, 2005.
[16] H. Bornfleth, P. Edelmann, D. Zink, T. Cremer, C. Cremer, "Quantitative motion analysis of subchromosomal foci in living cells using four-dimensional microscopy," *Biophysical Journal* 77(5):2871-2886, 1999.
[17] G. G. Cabal, A. Genovesio, S. Rodriguez-Navarro, C. Zimmer, O. Gadal, A. Lesne, H. Buc, F. Feuerbach-Fournier, J.-C. Olivo-Marin, E. C. Hurt, U. Nehrbass, "SAGA interacting factors confine sub-diffusion of transcribed genes to the nuclear envelope," *Nature* 441(7094):770-773, 2006.
[18] M. B. Cannell, A. McMorland, C. Soeller, "Image enhancement by deconvolution," in *Handbook of Biological Confocal Microscopy*, J. B. Pawley (ed.), Springer, New York, Ch. 25, pp. 488-500, 2006.
[19] D. W. Capson, R. A. Maludzinski, I. A. Feuerstein, "Microcomputer-based interactive tracking of blood cells at biomaterial surfaces," *IEEE Transactions on Biomedical Engineering* 36(8):860-864, 1989.
[20] B. C. Carter, G. T. Shubeita, S. P. Gross, "Tracking single particles: A user-friendly quantitative evaluation," *Physical Biology* 2(1):60-72, 2005.
[21] T. F. Chan, L. A. Vese, "Active contours without edges," *IEEE Transactions on Image Processing* 10(2):266-277, 2001.
[22] M. K. Cheezum, W. F. Walker, W. H. Guilford, "Quantitative comparison of algorithms for tracking single fluorescent particles," *Biophysical Journal* 81(4):2378-2388, 2001.
[23] X. Chen, X. Zhou, S. T. C. Wong, "Automated segmentation, classification, and tracking of cancer cell nuclei in time-lapse microscopy," *IEEE Transactions on Biomedical Engineering* 53(4):762-766, 2006.
[24] M. Chicurel, "Cell migration research is on the move," *Science* 295(5555):606-609, 2002.
[25] J. H. Chon, A. D. Vizena, B. M. Rock, E. L. Chaikof, "Characterization of single-cell migration using a computer-aided fluorescence time-lapse videomicroscopy system," *Analytical Biochemistry* 252(2):246-254, 1997.
[26] J. Cui, S. T. Acton, Z. Lin, "A Monte Carlo approach to rolling leukocyte tracking in vivo," *Medical Image Analysis* 10(4):598-610, 2006.
[27] O. Debeir, I. Camby, R. Kiss, P. Van Ham, C. Decaestecker, "A model-based approach for automated in vitro cell tracking and chemotaxis analyses," *Cytometry* 60A(1):29-40, 2004.
[28] O. Debeir, P. Van Ham, R. Kiss, C. Decaestecker, "Tracking of migrating cells under phase-contrast video microscopy with combined mean-shift processes," *IEEE Transactions on Medical Imaging* 24(6):697-711, 2005.
[29] Z. N. Demou, L. V. McIntire, "Fully automated three-dimensional tracking of cancer cells in collagen gels: Determination of motility phenotypes at the cellular level," *Cancer Research* 62(18):5301-5307, 2002.
[30] J. Deubler, J.-C. Olivo-Marin, "A wavelet-based multiresolution method to automatically register images," *Journal of Mathematical Imaging and Vision* 7(3):199-209, 1997.
[31] D. L. Donoho, "De-noising by soft-thresholding," *IEEE Transactions on Information Theory* 41(3):613-627, 1995.

[32] R. M. Donovan, E. Goldstein, Y. Kim, W. Lippert, A. T. W. Cheung, M. E. Miller, "A quantitative method for the analysis of cell shape and locomotion," *Histochemistry* 84(4-6):525-529, 1986.
[33] D. Dormann, T. Libotte, C. J. Weijer, T. Bretschneider, "Simultaneous quantification of cell motility and protein-membrane-association using active contours," *Cell Motility and the Cytoskeleton* 52(4):221-230, 2002.
[34] D. Dormann, C. J. Weijer, "Imaging of cell migration," *EMBO Journal* 25(15):3480-3493, 2006.
[35] J. F. Dorn, K. Jaqaman, D. R. Rines, G. S. Jelson, P. K. Sorger, G. Danuser, "Yeast kinetochore microtubule dynamics analyzed by high-resolution three-dimensional microscopy," *Biophysical Journal* 89(4):2835-2854, 2005.
[36] J. A. T. Dow, J. M. Lackie, K. V. Crocket, "A simple microcomputer-based system for real-time analysis of cell behavior," *Journal of Cell Science* 87(1):171-182, 1987.
[37] A. Dufour, V. Shinin, S. Tajbakhsh, N. Guillen-Aghion, J.-C. Olivo-Marin, C. Zimmer, "Segmenting and tracking fluorescent cells in dynamic 3-D microscopy with coupled active surfaces," *IEEE Transactions on Image Processing* 14(9):1396-1410, 2005.
[38] M. Dyba, S. Jakobs, S. W. Hell, "Immunofluorescence stimulated emission depletion microscopy," *Nature Biotechnology* 21(11):1303-1304, 2003.
[39] O. Dzyubachyk, W. Niessen, E. Meijering, "A variational model for level-set based cell tracking in time-lapse fluorescence microscopy images," *Proceedings of the IEEE International Symposium on Biomedical Imaging: From Nano to Macro*, IEEE, Piscataway, NJ, 2007.
[40] E. Eden, D. Waisman, M. Rudzsky, H. Bitterman, V. Brod, E. Rivlin, "An automated method for analysis of flow characteristics of circulating particles from in vivo video microscopy," *IEEE Transactions on Medical Imaging* 24(8):1011-1024, 2005.
[41] R. Eils, C. Athale, "Computational imaging in cell biology," *Journal of Cell Biology* 161(3):477-481, 2003.
[42] R. Fernández-González, A. Muñoz-Barrutia, M. H. Barcellos-Hoff, C. Ortiz-de-Solorzano, "Quantitative in vivo microscopy: The return from the 'omics'," *Current Opinion in Biotechnology* 17(5):501-510, 2006.
[43] R. Ferrari, A. J. Manfroi, W. R. Young, "Strongly and weakly self-similar diffusion," *Physica D* 154(1):111-137, 2001.
[44] F. P. Ferrie, M. D. Levine, S. W. Zucker, "Cell tracking: A modeling and minimization approach," *IEEE Transactions on Pattern Analysis and Machine Intelligence* 4(3):277-291, 1982.
[45] D. Gauthier, M. D. Levine, P. B. Noble, "Principles of object detection for an automated cell tracking system," in *Image Analysis in Biology*, D.-P. Häder (ed.), CRC Press, Boca Raton, Ch. 2, pp. 9-28, 1992.
[46] J. Gelles, B. J. Schnapp, M. P. Sheetz, "Tracking kinesin-driven movements with nanometre-scale precision," *Nature* 331(6155):450-453, 1988.
[47] A. Genovesio, T. Liedl, V. Emiliani, W. J. Parak, M. Coppey-Moisan, J.-C. Olivo-Marin, "Multiple particle tracking in 3-D+t microscopy: Method and application to the tracking of endocytosed quantum dots," *IEEE Transactions on Image Processing* 15(5):1062-1070, 2006.
[48] D. Gerlich, J. Beaudouin, M. Gebhard, J. Ellenberg, R. Eils, "Four-dimensional imaging and quantitative reconstruction to analyse complex spatiotemporal processes in live cells," *Nature Cell Biology* 3(9):852-855, 2001.
[49] D. Gerlich, J. Ellenberg, "4D imaging to assay complex dynamics in live specimens," *Nature Cell Biology* 5:S14-S19, 2003.
[50] D. Gerlich, J. Mattes, R. Eils, "Quantitative motion analysis and visualization of cellular structures," *Methods* 29(1):3-13, 2003.
[51] F. Germain, A. Doisy, X. Ronot, P. Tracqui, "Characterization of cell deformation and migration using a parametric estimation of image motion," *IEEE Transactions on Biomedical Engineering* 46(5):584-600, 1999.
[52] R. N. Ghosh, W. W. Webb, "Automated detection and tracking of individual and clustered cell surface low density lipoprotein receptor molecules," *Biophysical Journal* 66(5):1301-1318, 1994.
[53] A. P. Goobic, J. Tang, S. T. Acton, "Image stabilization and registration for tracking cells in the microvasculature," *IEEE Transactions on Biomedical Engineering* 52(2):287-299, 2005.
[54] M. Goulian, S. M. Simon, "Tracking single proteins within cells," *Biophysical Journal* 79(4):2188-2198, 2000.
[55] V. Grau, A. U. J. Mewes, M. Alcañiz, R. Kikinis, S. K. Warfield, "Improved watershed transform for medical image segmentation using prior information," *IEEE Transactions on Medical Imaging* 23(4):447-458, 2004.
[56] J. V. Hajnal, D. L. G. Hill, D. J. Hawkes, *Medical Image Registration*, CRC Press, Boca Raton, 2001.
[57] C. De Hauwer, F. Darro, I. Camby, R. Kiss, P. Van Ham, C. Decaestecker, "In vitro motility evaluation of aggregated cancer cells by means of automatic image processing," *Cytometry* 36(1):1-10, 1999.
[58] P. J. Heid, E. Voss, D. R. Soll, "3D-DIASemb: A computer-assisted system for reconstructing and motion analyzing in 4D every cell and nucleus in a developing embryo," *Developmental Biology* 245(2):329-347, 2002.
[59] S. W. Hell, "Toward fluorescence nanoscopy," *Nature Biotechnology* 21(11):1347-1355, 2003.
[60] S. W. Hell, M. Dyba, S. Jakobs, "Concepts for nanoscale resolution in fluorescence microscopy," *Current Opinion in Neurobiology* 14(5):599-609, 2004.
[61] D. L. G. Hill, P. G. Batchelor, M. Holden, D. J. Hawkes, "Medical image registration," *Physics in Medicine and Biology* 46(3):R1-R45, 2001.

[62] T. J. Holmes, D. Biggs, A. Abu-Tarif, "Blind deconvolution," in *Handbook of Biological Confocal Microscopy*, J. B. Pawley (ed.), Springer, New York, Ch. 24, pp. 468-487, 2006.
[63] A. Hoppe, D. Wertheim, W. G. Jiang, R. Williams, K. Harding, "Interactive image processing system for assessment of cell movement," *Medical & Biological Engineering & Computing* 37(4):419-423, 1999.
[64] R. van Horssen, N. Galjart, J. A. P. Rens, A. M. M. Eggermont, T. L. M. ten Hagen, "Differential effects of matrix and growth factors on endothelial and fibroblast motility: Application of a modified cell migration assay," *Journal of Cellular Biochemistry* 99(6):1536-1552, 2006.
[65] M. Isard, A. Blake, "CONDENSATION – Conditional density propagation for visual tracking," *International Journal of Computer Vision* 29(1):5-28, 1998.
[66] N. N. Kachouie, P. Fieguth, J. Ramunas, E. Jervis, "Probabilistic model-based cell tracking," *International Journal of Biomedical Imaging* 2006(12186):1-10, 2006.
[67] Z. Kam, B. Hanser, M. G. L. Gustafsson, D. A. Agard, J. W. Sedat, "Computational adaptive optics for live three-dimensional biological imaging," *Proceedings of the National Academy of Sciences of the United States of America* 98(7):3790-3795, 2001.
[68] M. Kass, A. Witkin, D. Terzopoulos, "Snakes: Active contour models," *International Journal of Computer Vision* 1(4):321-331, 1988.
[69] P. M. Kasson, J. B. Huppa, M. Krogsgaard, M. M. Davis, A. T. Brunger, "Quantitative imaging of lymphocyte membrane protein reorganization and signaling," *Biophysical Journal* 88(1):579-589, 2005.
[70] D. F. Katz, R. O. Davis, B. A. Delandmeter, J. W. Overstreet, "Real-time analysis of sperm motion using automatic video image digitization," *Computer Methods and Programs in Biomedicine* 21(3):173-182, 1985.
[71] D. J. E. B. Krooshoop, R. Torensma, G. J. M. van den Bosch, J. M. D. T. Nelissen, C. G. Figdor, R. A. P. Raymakers, J. B. M. Boezeman, "An automated multi well cell track system to study leukocyte migration," *Journal of Immunological Methods* 280(1-2):89-102, 2003.
[72] U. Kubitscheck, O. Kückmann, T. Kues, R. Peters, "Imaging and tracking of single GFP molecules in solution," *Biophysical Journal* 78(4):2170-2179, 2000.
[73] T. Kues, R. Peters, U. Kubitscheck, "Visualization and tracking of single protein molecules in the cell nucleus," *Biophysical Journal* 80(6):2954-2967, 2001.
[74] V. Levi, Q. Ruan, E. Gratton, "3-D particle tracking in a two-photon microscope: Application to the study of molecular dynamics in cells," *Biophysical Journal* 88(4):2919-2928, 2005.
[75] V. Levi, Q. Ruan, K. Kis-Petikova, E. Gratton, "Scanning FCS: A novel method for three-dimensional particle tracking," *Biochemical Society Transactions* 31(5):997-1000, 2003.
[76] M. D. Levine, Y. M. Youssef, P. B. Noble, A. Boyarsky, "The quantification of blood cell motion by a method of automatic digital picture processing," *IEEE Transactions on Pattern Analysis and Machine Intelligence* 2(5):444-450, 1980.
[77] F. Leymarie, M. D. Levine, "Tracking deformable objects in the plane using an active contour model," *IEEE Transactions on Pattern Analysis and Machine Intelligence* 15(6):617-634, 1993.
[78] D. Li, J. Xiong, A. Qu, T. Xu, "Three-dimensional tracking of single secretory granules in live PC12 cells," *Biophysical Journal* 87(3):1991-2001, 2004.
[79] G. Lin, U. Adiga, K. Olson, J. F. Guzowski, C. A. Barnes, B. Roysam, "A hybrid 3D watershed algorithm incorporating gradient cues and object models for automatic segmentation of nuclei in confocal image stacks," *Cytometry* 56A(1):23-36, 2003.
[80] J. Lippincott-Schwartz, N. Altan-Bonnet, G. H. Patterson, "Photobleaching and photoactivation: Following protein dynamics in living cells," *Nature Cell Biology* 5:S7-S13, 2003.
[81] J. Lippincott-Schwartz, G. H. Patterson, "Development and use of fluorescent protein markers in living cells," *Science* 300(5616):87-91, 2003.
[82] Y. T. Liu, P. K. Warme, "Computerized evaluation of sperm cell motility," *Computers and Biomedical Research* 10(2):127-138, 1977.
[83] M. Machin, A. Santomaso, M. Mazzucato, M. Rita Cozzi, M. Battiston, L. De Marco, P. Canu, "Single particle tracking across sequences of microscopical images: Application to platelet adhesion under flow," *Annals of Biomedical Engineering* 34(5):833-846, 2006.
[84] S. O. Mack, D. P. Wolf, J. S. Tash, "Quantitation of specific parameters of motility in large numbers of human sperm by digital image processing," *Biology of Reproduction* 38(2):270-281, 1988.
[85] J. B. A. Maintz, M. A. Viergever, "A survey of medical image registration," *Medical Image Analysis* 2(1):1-36, 1998.
[86] N. Malpica, C. O. de Solórzano, J. J. Vaquero, A. Santos, I. Vallcorba, J. M. García-Sagredo, F. del Pozo, "Applying watershed algorithms to the segmentation of clustered nuclei," *Cytometry* 28(4):289-297, 1997.
[87] R. A. Maludzinski, D. W. Capson, I. A. Feuerstein, "Computer tracking of white blood cells on protein-coated surfaces," *IEEE Transactions on Instrumentation and Measurement* 36(4):928-933, 1987.

[88] S. B. Marston, I. D. C. Fraser, W. Bing, G. Roper, "A simple method for automatic tracking of actin filaments in the motility assay," *Journal of Muscle Research and Cell Motility* 17(4):497-506, 1996.
[89] D. S. Martin, M. B. Forstner, J. A. Käs, "Apparent subdiffusion inherent to single particle tracking," *Biophysical Journal* 83(4):2109-2117, 2002.
[90] T. Matthes, H. Gruler, "Analysis of cell locomotion. Contact guidance of human polymorphonuclear leukocytes," *European Biophysics Journal* 15(6):343-357, 1988.
[91] M. McCutcheon, "Chemotaxis in leukocytes," *Physiological Reviews* 26(3):319-336, 1946.
[92] T. McInerney, D. Terzopoulos, "Deformable models in medical image analysis: A survey," *Medical Image Analysis* 1(2):91-108, 1996.
[93] E. Meijering, I. Smal, G. Danuser, "Tracking in molecular bioimaging," *IEEE Signal Processing Magazine* 23(3):46-53, 2006.
[94] K. Miura, "Tracking movement in cell biology," in *Microscopy Techniques*, J. Rietdorf (ed.), vol. 95 of *Advances in Biochemical Engineering/Biotechnology*, Springer-Verlag, Berlin, Ch. 10, pp. 267-295, 2005.
[95] A. Miyawaki, A. Sawano, T. Kogure, "Lighting up cells: Labelling proteins with fluorophores," *Nature Cell Biology* 5:S1-S7, 2003.
[96] D. P. Mukherjee, N. Ray, S. T. Acton, "Level set analysis for leukocyte detection and tracking," *IEEE Transactions on Medical Imaging* 13(4):562-572, 2004.
[97] R. F. Murphy, E. Meijering, G. Danuser, "Special issue on molecular and cellular bioimaging," *IEEE Transactions on Image Processing* 14(9):1233-1236, 2005.
[98] R. J. Ober, S. Ram, E. S. Ward, "Localization accuracy in single-molecule microscopy," *Biophysical Journal* 86(2):1185-1200, 2004.
[99] J.-C. Olivo-Marin, "Extraction of spots in biological images using multiscale products," *Pattern Recognition* 35(9):1989-1996, 2002.
[100] J. B. Pawley (ed.), *Handbook of Biological Confocal Microscopy*, 3rd ed., Springer, New York, 2006.
[101] P. Perona, J. Malik, "Scale-space and edge detection using anisotropic diffusion," *IEEE Transactions on Pattern Analysis and Machine Intelligence* 12(7):629–639, 1990.
[102] J. P. W. Pluim, J. B. A. Maintz, M. A. Viergever, "Mutual-information-based registration of medical images: A survey," *IEEE Transactions on Medical Imaging* 22(8):986-1004, 2003.
[103] N. Pouget, C. Dennis, C. Turlan, M. Grigoriev, M. Chandler, L. Salomé, "Single-particle tracking for DNA tether length monitoring," *Nucleic Acids Research* 32(9):e73, 2004.
[104] H. Qian, M. P. Sheetz, E. L. Elson, "Single particle tracking: Analysis of diffusion and flow in two-dimensional systems," *Biophysical Journal* 60(4):910-921, 1991.
[105] X. Qu, D. Wu, L. Mets, N. F. Scherer, "Nanometer-localized multiple single-molecule fluorescence microscopy," *Proceedings of the National Academy of Sciences of the United States of America* 101(31):11298-11303, 2004.
[106] G. Rabut, J. Ellenberg, "Automatic real-time three-dimensional cell tracking by fluorescence microscopy," *Journal of Microscopy* 216(2):131-137, 2004.
[107] T. Ragan, H. Huang, P. So, E. Gratton, "3D particle tracking on a two-photon microscope," *Journal of Fluorescence* 16(3):325-336, 2006.
[108] S. Ram, E. S. Ward, R. J. Ober, "Beyond Rayleigh's criterion: A resolution measure with application to single-molecule microscopy," *Proceedings of the National Academy of Sciences of the United States of America* 103(12):4457-4462, 2006.
[109] N. Ray, S. T. Acton, "Motion gradient vector flow: An external force for tracking rolling leukocytes with shape and size constrained active contours," *IEEE Transactions on Medical Imaging* 23(12):1466-1478, 2004.
[110] N. Ray, S. T. Acton, "Data acceptance for automated leukocyte tracking through segmentation of spatiotemporal images," *IEEE Transactions on Biomedical Engineering* 52(10):1702-1712, 2005.
[111] N. Ray, S. T. Acton, K. Ley, "Tracking leukocytes in vivo with shape and size constrained active contours," *IEEE Transactions on Medical Imaging* 21(10):1222-1235, 2002.
[112] B. Rieger, C. Molenaar, R. W. Dirks, L. J. van Vliet, "Alignment of the cell nucleus from labeled proteins only for 4D in vivo imaging," *Microscopy Research and Technique* 64(2):142-150, 2004.
[113] M. J. Rust, M. Bates, X. Zhuang, "Sub-diffraction-limit imaging by stochastic optical reconstruction microscopy (STORM)," *Nature Methods* 3(10):793-795, 2006.
[114] S. Sabri, F. Richelme, A. Pierres, A.-M. Benoliel, P. Bongrand, "Interest of image processing in cell biology and immunology," *Journal of Immunological Methods* 208(1):1-27, 1997.
[115] D. Sage, F. R. Neumann, F. Hediger, S. M. Gasser, M. Unser, "Automatic tracking of individual fluorescence particles: Application to the study of chromosome dynamics," *IEEE Transactions on Image Processing* 14(9):1372-1383, 2005.
[116] P. Sarder, A. Nehorai, "Deconvolution methods for 3-D fluorescence microscopy images," *IEEE Signal Processing Magazine* 23(3):32-45, 2006.

[117] A. Sarti, C. Ortiz de Solórzano, S. Lockett, R. Malladi, "A geometric model for 3-D confocal image analysis," *IEEE Transactions on Biomedical Engineering* 47(12):1600-1609, 2000.
[118] Y. Sato, J. Chen, R. A. Zoroofi, N. Harada, S. Tamura, T. Shiga, "Automatic extraction and measurement of leukocyte motion in microvessels using spatiotemporal image analysis," *IEEE Transactions on Biomedical Engineering* 44(4):225-236, 1997.
[119] M. J. Saxton, K. Jacobson, "Single-particle tracking: Applications to membrane dynamics," *Annual Review of Biophysics and Biomolecular Structure* 26:373-399, 1997.
[120] I. F. Sbalzarini, P. Koumoutsakos, "Feature point tracking and trajectory analysis for video imaging in cell biology," *Journal of Structural Biology* 151(2):182-195, 2005.
[121] J. Serra, *Image Analysis and Mathematical Morphology*, Academic Press, London, 1982.
[122] J. A. Sethian, *Level Set Methods and Fast Marching Methods: Evolving Interfaces in Computational Geometry, Fluid Mechanics, Computer Vision, and Materials Science*, Cambridge University Press, New York, 1999.
[123] C. E. Shannon, "Communication in the presence of noise," *Proceedings of the Institution of Radio Engineers* 37(1):10-21, 1949.
[124] H. Shen, G. Nelson, S. Kennedy, D. Nelson, J. Johnson, D. Spiller, M. R. H. White, D. B. Kell, "Automatic tracking of biological cells and compartments using particle filters and active contours," *Chemometrics and Intelligent Laboratory Systems* 82(1-2):276-282, 2006.
[125] C. J. R. Sheppard, X. Gan, M. Gu, M. Roy, "Signal-to-noise ratio in confocal microscopes," in *Handbook of Biological Confocal Microscopy*, J. B. Pawley (ed.), 3rd ed., Springer, New York, Ch. 22, pp. 442-452, 2006.
[126] L. Z. Shi, J. Nascimento, C. Chandsawangbhuwana, M. W. Berns, E. L. Botvinick, "Real-time automated tracking and trapping system for sperm," *Microscopy Research and Technique* 69(11):894-902, 2006.
[127] F. Siegert, C. J. Weijer, A. Nomura, H. Miike, "A gradient method for the quantitative analysis of cell movement and tissue flow and its application to the analysis of multicellular Dictyostelium development," *Journal of Cell Science* 107(1):97-104, 1994.
[128] I. Smal, W. Niessen, E. Meijering, "Advanced particle filtering for multiple object tracking in dynamic fluorescence microscopy images," *Proceedings of the IEEE International Symposium on Biomedical Imaging: From Nano to Macro*, IEEE, Piscataway, NJ, 2007.
[129] D. R. Soll, "The use of computers in understanding how animal cells crawl," *International Review of Cytology* 163:43-104, 1995.
[130] C. Ortiz de Solórzano, E. García Rodriguez, A. Jones, D. Pinkel, J. W. Gray, D. Sudar, S. J. Lockett, "Segmentation of confocal microscope images of cell nuclei in thick tissue sections," *Journal of Microscopy* 193(3):212-226, 1999.
[131] C. Ó. S. Sorzano, P. Thévenaz, M. Unser, "Elastic registration of biological images using vector-spline regularization," *IEEE Transactions on Biomedical Engineering* 52(4):652-663, 2005.
[132] T. Stepanova, J. Slemmer, C. C. Hoogenraad, G. Lansbergen, B. Dortland, C. I. de Zeeuw, F. Grosveld, G. van Cappellen, A. Akhmanova, N. Galjart, "Visualization of microtubule growth in cultured neurons via the use of EB3-GFP (end-binding protein 3-green fluorescent protein)," *Journal of Neuroscience* 23(7):2655-2664, 2003.
[133] D. J. Stephens, V. J. Allan, "Light microscopy techniques for live cell imaging," *Science* 300(5616):82-86, 2003.
[134] J. Suh, M. Dawson, J. Hanes, "Real-time multiple-particle tracking: Application to drug and gene delivery," *Advanced Drug Delivery Reviews* 57(1):63-78, 2005.
[135] D. Thomann, J. Dorn, P. K. Sorger, G. Danuser, "Automatic fluorescent tag localization II: Improvement in super-resolution by relative tracking," *Journal of Microscopy* 211(3):230-248, 2003.
[136] D. Thomann, D. R. Rines, P. K. Sorger, G. Danuser, "Automatic fluorescent tag detection in 3D with super-resolution: Application to the analysis of chromosome movement," *Journal of Microscopy* 208(1):49-64, 2002.
[137] C. Thomas, P. DeVries, J. Hardin, J. White, "Four-dimensional imaging: Computer visualization of 3D movements in living specimens," *Science* 273(5275):603-607, 1996.
[138] R. E. Thompson, D. R. Larson, W. W. Webb, "Precise nanometer localization analysis for individual fluorescent probes," *Biophysical Journal* 82(5):2775-2783, 2002.
[139] G. Thurston, B. Jaggi, B. Palcic, "Measurement of cell motility and morphology with an automated microscope system," *Cytometry* 9(5):411-417, 1988.
[140] Y. Tseng, T. P. Kole, D. Wirtz, "Micromechanical mapping of live cells by multiple-particle-tracking microrheology," *Biophysical Journal* 83(6):3162-3176, 2002.
[141] Y. Tseng, J. S. H. Lee, T. P. Kole, I. Jiang, D. Wirtz, "Micro-organization and visco-elasticity of the interphase nucleus revealed by particle nanotracking," *Journal of Cell Science* 117(10):2159-2167, 2004.
[142] R. Y. Tsien, "Imagining imaging's future," *Nature Cell Biology* 5:S16-S21, 2003.
[143] W. Tvaruskó, M. Bentele, T. Misteli, R. Rudolf, C. Kaether, D. L. Spector, H. H. Gerdes, R. Eils, "Time-resolved analysis and visualization of dynamic processes in living cells," *Proceedings of the National Academy of Sciences of the United States of America* 96(14):7950-7955, 1999.

[144] D. Uttenweiler, C. Veigel, R. Steubing, C. Götz, S. Mann, H. Haussecker, B. Jähne, R. H. A. Fink, "Motion determination in actin filament fluorescence images with a spatio-temporal orientation analysis method," *Biophysical Journal* 78(5):2709-2715, 2000.
[145] D. Uttenweiler, C. Weber, B. Jähne, R. H. A. Fink, H. Scharr, "Spatiotemporal anisotropic diffusion filtering to improve signal-to-noise ratios and object restoration in fluorescence microscopic image sequences," *Journal of Biomedical Optics* 8(1):40-47, 2003.
[146] P. Vallotton, A. Ponti, C. M. Waterman-Storer, E. D. Salmon, G. Danuser, "Recovery, visualization, and analysis of actin and tubulin polymer flow in live cells: A fluorescent speckle microscopy study," *Biophysical Journal* 85(2):1289-1306, 2003.
[147] J. Vermaak, A. Doucet, P. Perez, "Maintaining multimodality through mixture tracking," *Proceedings of the Ninth IEEE International Conference on Computer Vision*, vol. 2, pp. 1110-1116, 2003.
[148] L. Vincent, P. Soille, "Watersheds in digital spaces: An efficient algorithm based on immersion simulations," *IEEE Transactions on Pattern Analysis and Machine Intelligence* 13(6):583-598, 1991.
[149] L. J. van Vliet, D. Sudar, I. T. Young, "Digital fluorescence imaging using cooled CCD array cameras," in *Cell Biology: A Laboratory Handbook*, J. E. Celis (ed.) vol. III, Academic Press, New York, NY, pp. 109-120, 1998.
[150] C. Vonesch, F. Aguet, J.-L. Vonesch, M. Unser, "The colored revolution of bioimaging," *IEEE Signal Processing Magazine* 23(3):20-31, 2006.
[151] C. Wählby, I.-M. Sintorn, F. Erlandsson, G. Borgefors, E. Bengtsson, "Combining intensity, edge and shape information for 2D and 3D segmentation of cell nuclei in tissue sections," *Journal of Microscopy* 215(1):67-76, 2004.
[152] D. J. Webb, A. F. Horwitz, "New dimensions in cell migration," *Nature Cell Biology* 5(8):690-692, 2003.
[153] D. Wessels, E. Voss, N. Von Bergen, R. Burns, J. Stites, D. R. Soll, "A computer-assisted system for reconstructing and interpreting the dynamic three-dimensional relationships of the outer surface, nucleus and pseudopods of crawling cells," *Cell Motility and the Cytoskeleton* 41(3):225-246, 1998.
[154] N. Wick, S. Thurner, K. Paiha, R. Sedivy, I. Vietor, L. A. Huber, "Quantitative measurement of cell migration using time-lapse videomicroscopy and non-linear system analysis," *Histochemistry and Cell Biology* 119(1):15-20, 2003.
[155] C. A. Wilson, J. A. Theriot, "A correlation-based approach to calculate rotation and translation of moving cells," *IEEE Transactions on Image Processing* 15(7):1939-1951, 2006.
[156] S. S. Work, D. M. Warshaw, "Computer-assisted tracking of actin filament motility," *Analytical Biochemistry* 202(2):275-285, 1992.
[157] K. Wu, D. Gauthier, M. D. Levine, "Live cell image segmentation," *IEEE Transactions on Biomedical Engineering* 42(1):1-12, 1995.
[158] C. Xu, J. L. Prince, "Snakes, shapes, and gradient vector flow," *IEEE Transactions on Image Processing* 7(3):359-369, 1998.
[159] X. Yang, H. Li, X. Zhou, "Nuclei segmentation using marker-controlled watershed, tracking using mean-shift, and Kalman filter in time-lapse microscopy," *IEEE Transactions on Circuits and Systems I: Regular Papers* 53(11):2405-2414, 2006.
[160] I. T. Young, "Image fidelity: Characterizing the imaging transfer function," in *Fluorescence Microscopy of Living Cells in Culture. Part B: Quantitative Fluorescence Microscopy – Imaging and Spectroscopy*, D. L. Taylor, Y.-L. Wang (eds.), vol. 30 of *Methods in Cell Biology*, Academic Press, San Diego, CA, Ch. 1, pp. 1-45, 1989.
[161] D. Young, C. A. Glasbey, A. J. Gray, N. J. Martin, "Towards automatic cell identification in DIC microscopy," *Journal of Microscopy* 192(2):186-193, 1998.
[162] S. T. Young, W. L. Tzeng, Y. L. Kuo, M. L. Hsiao, S. R. Chiang, "Real-time tracing of spermatozoa," *IEEE Engineering in Medicine and Biology Magazine* 15(6):117-120, 1996.
[163] B. Zhang, J. Zerubia, J.-C. Olivo-Marin, "Gaussian approximations of fluorescence microscope point-spread function models," *Applied Optics* 46(10):1819-1829, 2007.
[164] C. Zimmer, E. Labruyère, V. Meas-Yedid, N. Guillén, J.-C. Olivo-Marin, "Segmentation and tracking of migrating cells in videomicroscopy with parametric active contours: A tool for cell-based drug testing," *IEEE Transactions on Medical Imaging* 21(10):1212-1221, 2002.
[165] C. Zimmer, J.-C. Olivo-Marin, "Coupled parametric active contours," *IEEE Transactions on Pattern Analysis and Machine Intelligence* 27(11):1838-1842, 2005.
[166] C. Zimmer, B. Zhang, A. Dufour, A. Thébaud, S. Berlemont, V. Meas-Yedid, J.-C. Olivo-Marin, "On the digital trail of mobile cells," *IEEE Signal Processing Magazine* 23(3):54-62, 2006.

Ref	Dim	Segmentation	Association	Microscopy	Application	Auto
[1]	2D+t	Manual indication	Template matching	PC	Leukocytes	MI
[8]	3D+t	Multiple thresholding	Template matching	F	Dictyostelium discoideum	FA
[23]	2D+t	Otsu thresholding + watersheds	Distance + area + overlap	F	HeLa cells	FA
[26]	2D+t	Manual indication + edges	Monte Carlo tracking	PC	Leukocytes	MI
[27]	2D+t	Manual indication + active contours	Active contour evolution	PC	Endothelial cells	MI
[28]	2D+t	Manual indication	Coupled mean shift processes	PC	Cancer and endothelial cells	MI
[29]	3D+t	Thresholding	Nearest cell	HMC	Cancer cells	FA
[33]	2D+t	Active contours	Active contour evolution	F	Dictyostelium cells	FA
[37]	3D+t	Multiple level sets	Level set evolution	F	Entamoeba histolytica and epithelial cells	FA
[57]	2D+t	Manual outlining + watersheds	Unknown matching algorithm	PC	PC-3 cells	MI
[66]	2D+t	Template matching	Probabilistic association	PC	Hematopoietic stem cells	FA
[71]	2D+t	Manual indication	Template matching	PC	HSB-2 T-cells	MI
[77]	2D+t	Manual outlining	Active contour evolution	BF	Fibroblasts	MI
[96]	2D+t	Level sets	Level set evolution	PC	Leukocytes	FA
[111]	2D+t	Manual indication	Contour evolution + Kalman filtering	PC	Leukocytes	MI
[118]	2D+t	Space-time filtering + thresholding	Space-time trace angle + distance	PC	Leukocytes	FA
[124]	2D+t	Active contours	Monte Carlo tracking	F	HeLa cells	FA
[155]	2D+t	Manual outlining + active contour	Fourier-based template matching	PC	Keratocytes	MI
[159]	2D+t	Marker controlled watersheds	Mean shift + Kalman filtering	F	HeLa cells	FA
[164]	2D+t	Manual outlining	Active contour evolution	PC	Entamoeba histolytica	MI

Table 1. Selected cell tracking methods and some of their features and applications. From left to right the columns indicate the reference number describing the method, the dimensionality of the data for which the method was designed, the main features of spatial segmentation and temporal association used by the method, the type of microscopy used and the applications considered in the described experiments, and the level of automation of the method. BF = brightfield. F = fluorescence. FA = fully automatic, meaning that in principle no user interaction is required, other than parameter tuning. HMC = Hoffman modulation contrast. MI = manual initialization, meaning that more user interaction is required than parameter tuning. PC = phase contrast.

Ref	Dim	Detection	Association	Microscopy	Application	Auto
[4]	2D+t	Gaussian fitting	Distance + intensity	F	Lipoproteins, influenza viruses	FA
[6]	2D+t	Thresholding + centroid	Nearest particle	F	Microspheres, actin filaments	FA
[9]	3D+t	Pyramid linking	Intensity + velocity + acceleration	F	Microspheres, vimentin	FA
[15]	2D+t	Template matching	Minimum cost paths	F	Quantum dots, glycine receptors	FA
[16]	3D+t	Thresholding + centroid	Template matching	F	Subchromosomal foci	FA
[35]	3D+t	Gaussian mixture fitting	Template matching	F	Kinetochore microtubules	FA
[40]	2D+t	Artificial neural networks	Velocity and virtual flow	F	Microspheres	FA
[47]	3D+t	Multiscale products	Interacting multiple models	F	Quantum dots, endocytic vesicles	FA
[48]	3D+t	Thresholding	Fuzzy logic	F	Chromosomes, centrosomes	FA
[52]	2D+t	Thresholding + centroid	Nearest particle	F	Low density lipoprotein receptors	FA
[54]	2D+t	Local maxima	Nearest particle	F	R-phycoerythrin	FA
[73]	2D+t	Gaussian fitting	Nearest particle	F	P4K proteins	FA
[78]	3D+t	Thresholding + centroid	Nearest particle	F	Secretory granules	FA
[88]	2D+t	Thresholding + centroid	Nearest particle	F	Actin filaments	FA
[115]	3D+t	Laplacian of Gaussian	Dynamic programming	F	Telomeres	FA
[120]	2D+t	Local maxima	Distance + intensity moments	TIRF	Lipoproteins, adenovirus-2, quantum dots	FA
[136]	3D+t	Gaussian mixture fitting	Global weighted distance minimization	F	Chromosomes, spindle pole body	FA
[143]	2D+t	Gradient magnitude + tracing	Fuzzy logic	F	Secretory vesicles, speckles	FA
[146]	2D+t	Local maxima selection	Multilayered graphs	F	Actin and tubulin fluorescent speckles	FA
[156]	2D+t	Thresholding + centroid	Area + major/minor axes + distance	F	Actin filaments	FA

Table 2. Selected particle tracking methods and some of their features and applications. From left to right the columns indicate the reference number describing the method, the dimensionality of the data for which the method was designed, the main features of spatial detection and temporal association used by the method, the type of microscopy used and the applications considered in the described experiments, and the level of automation of the method. F = fluorescence. FA = fully automatic, meaning that in principle no user interaction is required, other than parameter tuning. TIRF = total internal reflection fluorescence.

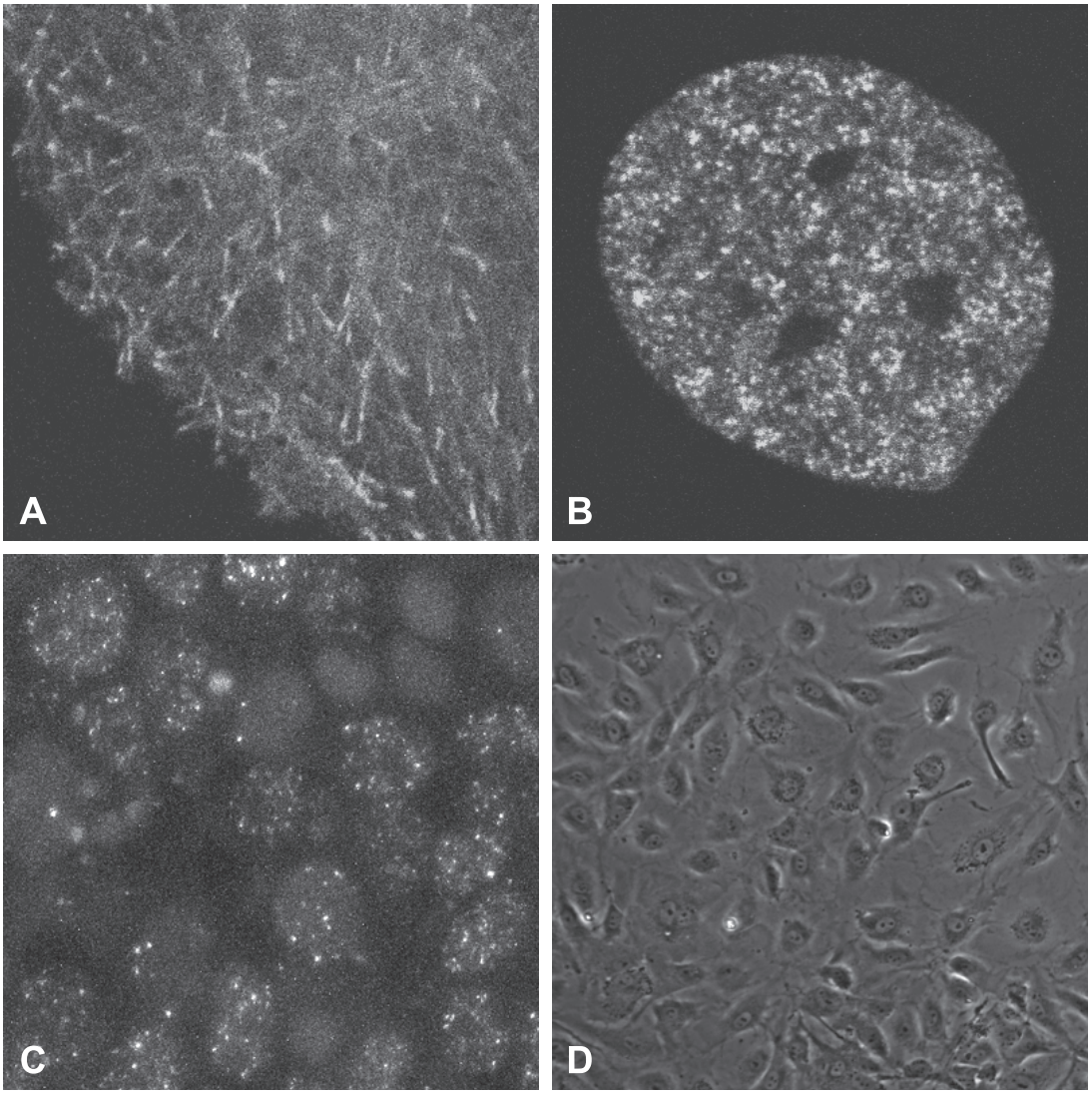

Figure 1. Sample frames from image sequences acquired for specific time-lapse imaging studies. The sequences contain large numbers of cells or subcellular particles to be tracked over time. A: Single frame (36×36 micron) from a fluorescence microscopy image sequence (1 sec. between frames) showing labeled microtubule plus-ends moving in the cytoplasm of a single COS-7 cell (only partly visible). B: Single frame (30×30 micron) from a fluorescence microscopy image sequence (about 12 sec. between frames) showing labeled androgen receptors moving in the nucleus of a Hep3B cell. C: Single frame (73×73 micron) from a fluorescence microscopy image sequence (about 16 min. between frames) showing labeled Rad54 proteins in the nuclei of mouse embryonic stem cells. D: Single frame (about 500×500 micron) from a phase-contrast microscopy image sequence (12 min. between frames) showing migrating human umbilical vein endothelial cells in a wound healing assay. Together, these examples show the complexity of typical time-lapse imaging data and the need for automated image analysis, but at the same time they illustrate the difficulty of the problem.

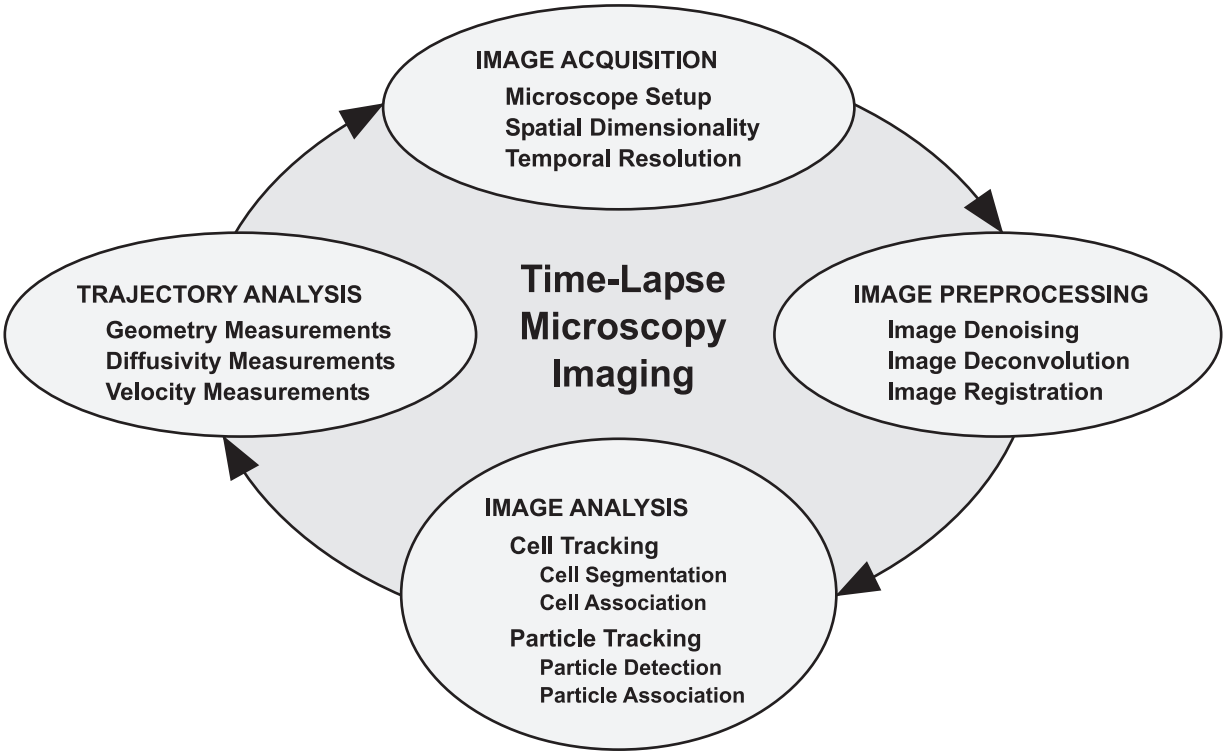

Figure 2. The circle of life in time-lapse microscopy imaging. The diagram depicts the successive steps in the imaging process and, at the same time, gives an overview of the topics addressed in this chapter. Following image acquisition, preprocessing is often required to increase the success of subsequent automated analysis of the images and, eventually, of the resulting trajectories. The circular structure of the diagram reflects the iterative nature of the imaging process: the results of previous experiments usually trigger the planning of new experiments.

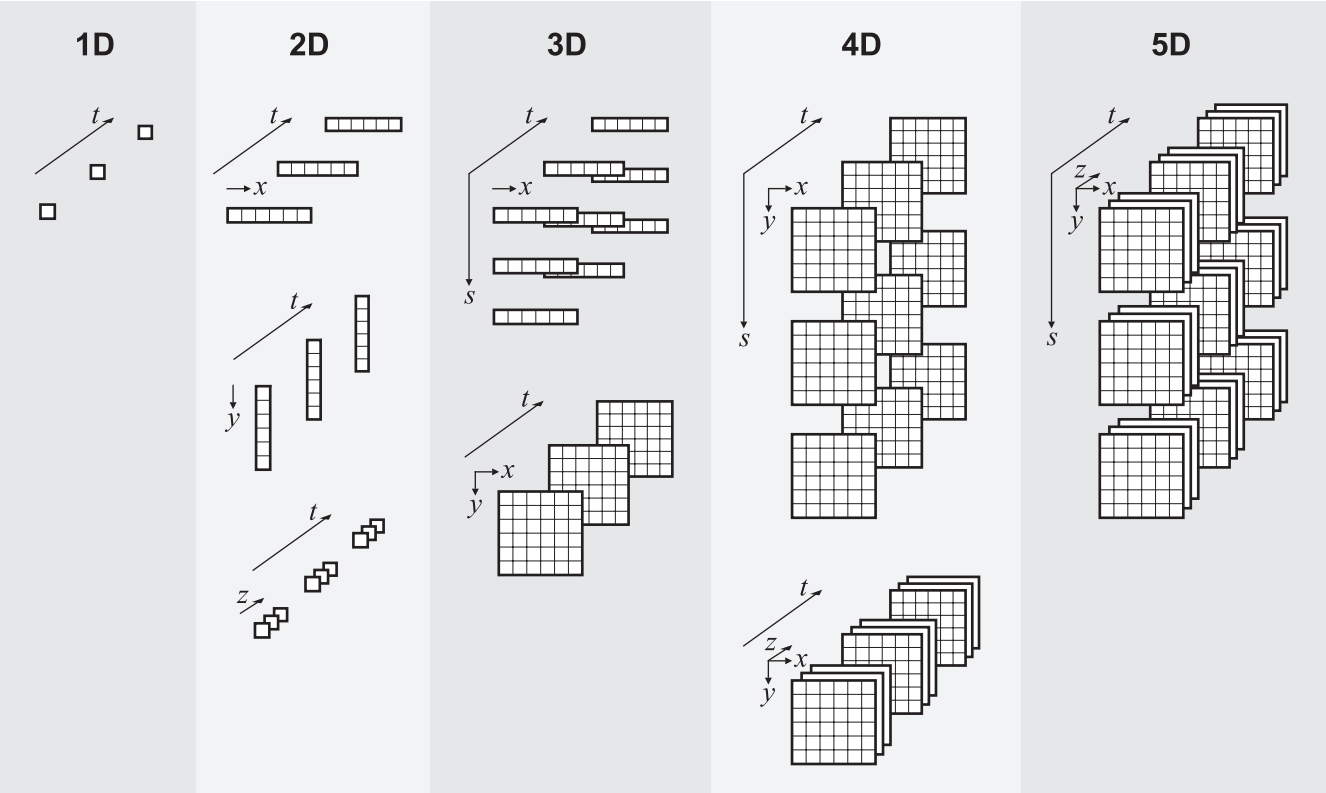

Figure 3. Possible image configurations and dimensionalities in time-lapse microscopy imaging. Each dimension corresponds to an independent physical parameter or coordinate: x and y commonly denote the in-plane spatial coordinates, z the depth or axial coordinate, t the time coordinate, and here s denotes any spectral parameter, such as wavelength. Notice that dimensionality, as used above, does not necessarily describe the image configuration unambiguously. For example, 4D imaging may refer to spatially 2D multispectral time-lapse imaging, or to spatially 3D time-lapse imaging. To avoid confusion, it is better to use the abbreviations 2D and 3D for referring to spatial dimensionality only, and to indicate explicitly whether the data also involves a temporal or spectral coordinate. Therefore, in this chapter, we indicate spatially 2D and 3D time-lapse imaging by 2D+t and 3D+t, respectively, rather than by 3D and 4D.

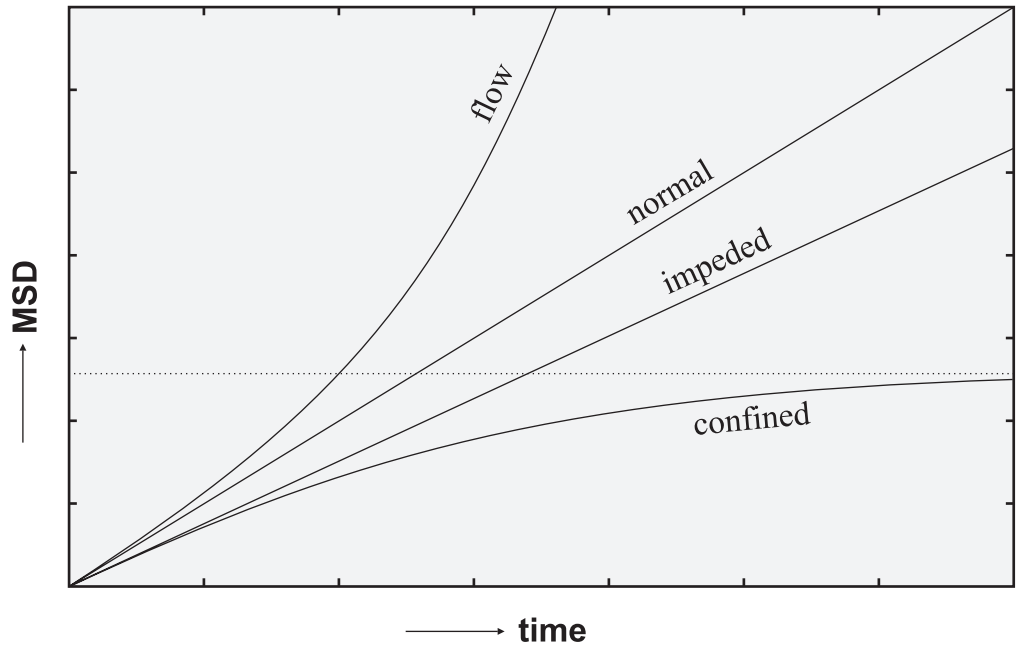

Figure 4. Different types of diffusivity characterized by the MSD as a function of time lag. The idealized curves apply to the case of noise-free measurements and consistent object motion. In the case of localization errors and non-consistent motion, the curves will show offsets and irregularities.

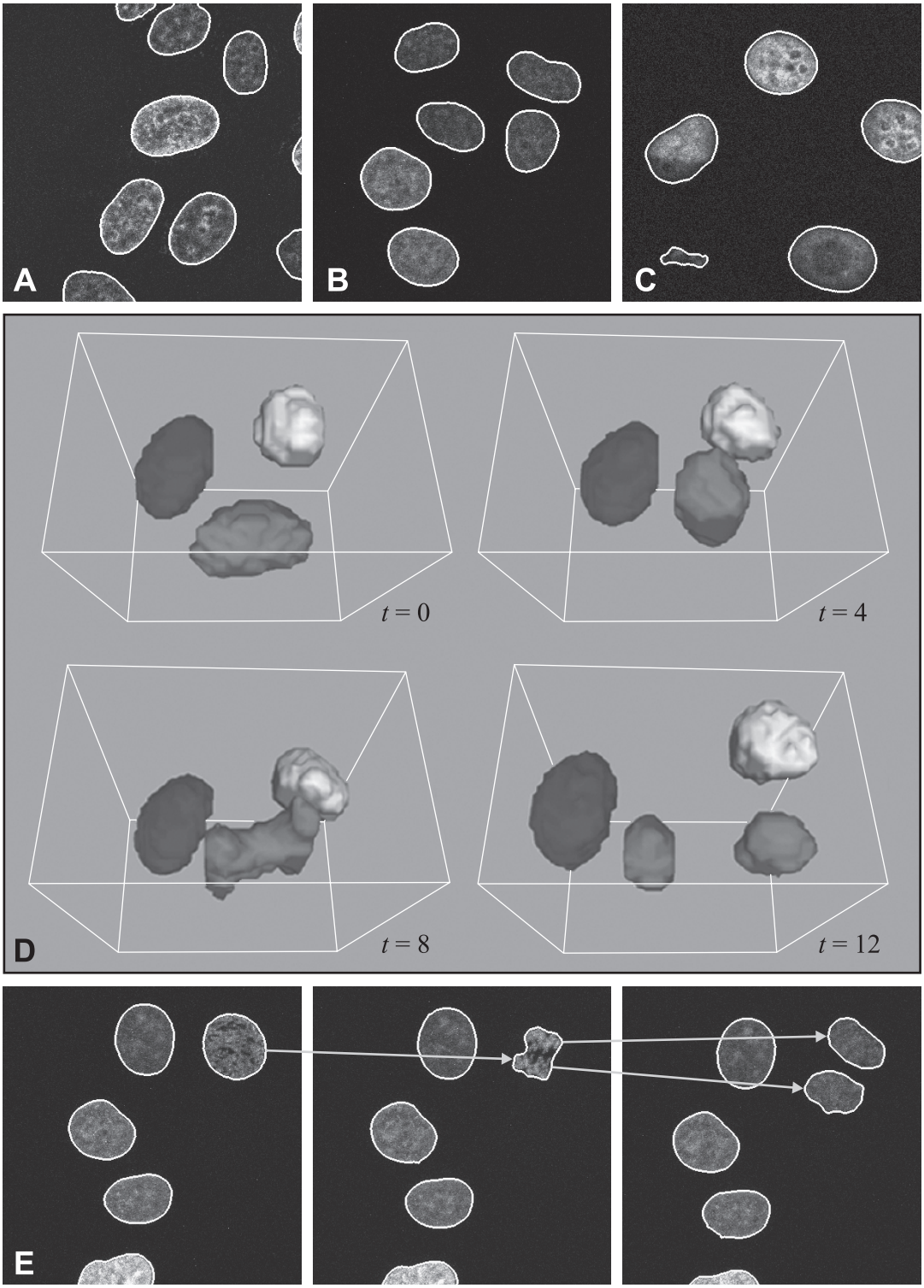

Figure 5. Sample results from applying the described level-set based cell tracking algorithm. A-C: Segmentations (white contours) for arbitrary frames taken from three different 2D+t image sequences. The examples illustrate the ability of the algorithm to yield plausible contours even in the presence of considerable object noise and strongly varying intensities, as caused, for example, by photobleaching in the case of FRAP experiments. D: Visualization of segmented surfaces of cell nuclei in four frames of a 3D+t image sequence. The renderings demonstrate the ability of the algorithm to keep track of cell division. E: Illustration of tracking cell division in a 2D+t image sequence.

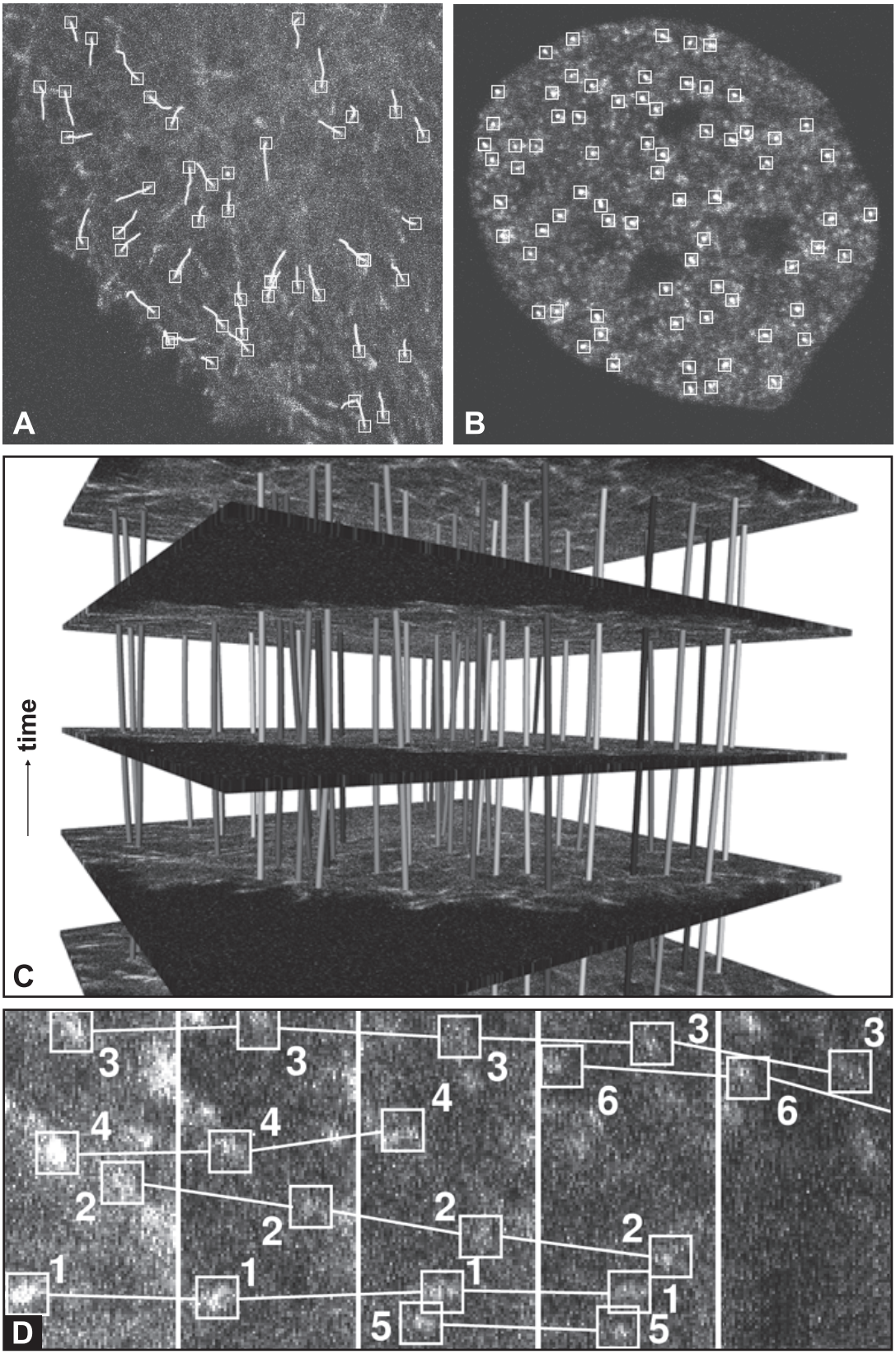

Figure 6. Sample results from applying the described SMC-based particle tracking algorithm. A and B: Estimated current locations (white squares) and trajectories (white curves) up to the current time, for the most prominent particles in an arbitrary frame from the 2D+t image sequences shown in Figure 1A and 1B, respectively. The trajectories in B are due to Brownian motion and are therefore strongly confined. C: Artistic rendering of the trajectories linking multiple frames of data set A. D: Illustration of the capability of the algorithm to deal with photobleaching, to capture newly appearing particles, detect particle disappearance, and handle closely passing particles.